

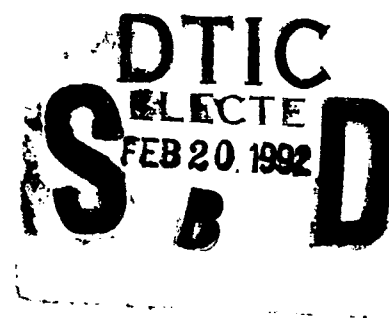
AD-A246 389



# NAVAL POSTGRADUATE SCHOOL

## Monterey, California

2



## THESIS

MODELING FOR IMPROVED  
MINIMUM RESOLVABLE TEMPERATURE DIFFERENCE  
MEASUREMENTS

by

Alejandro R. Ugarte

September, 1991

Thesis Advisor:

R. J. Pieper

Approved for public release; distribution is unlimited

92 2 14 16

92-03972



REPORT DOCUMENTATION PAGE				
1a. REPORT SECURITY CLASSIFICATION Unclassified			1b. RESTRICTIVE MARKINGS	
2a. SECURITY CLASSIFICATION AUTHORITY			3. DISTRIBUTION/AVAILABILITY OF REPORT Approved for public release; distribution is unlimited.	
2b. DECLASSIFICATION/DOWNGRADING SCHEDULE				
4. PERFORMING ORGANIZATION REPORT NUMBER(S)			5. MONITORING ORGANIZATION REPORT NUMBER(S)	
6a. NAME OF PERFORMING ORGANIZATION Naval Postgraduate School		6b. OFFICE SYMBOL (If applicable) EC	7a. NAME OF MONITORING ORGANIZATION Naval Postgraduate School	
6c. ADDRESS (City, State, and ZIP Code) Monterey, CA 93943-5000			7b. ADDRESS (City, State, and ZIP Code) Monterey, CA 93943-5000	
8a. NAME OF FUNDING/SPONSORING ORGANIZATION		8b. OFFICE SYMBOL (If applicable)	9. PROCUREMENT INSTRUMENT IDENTIFICATION NUMBER	
8c. ADDRESS (City, State, and ZIP Code)			10. SOURCE OF FUNDING NUMBERS	
			Program Element No	Project No
			Task No	Work Unit Accession Number
11. TITLE (Include Security Classification) MODELING FOR IMPROVED MINIMUM RESOLVABLE TEMPERATURE DIFFERENCE MEASUREMENTS				
12. PERSONAL AUTHOR(S) Ugarte, Alejandro R.				
13a. TYPE OF REPORT Master's Thesis		13b. TIME COVERED From To	14. DATE OF REPORT (year, month, day) 1991 September	15. PAGE COUNT 105
16. SUPPLEMENTARY NOTATION The views expressed in this thesis are those of the author and do not reflect the official policy or position of the Department of Defense or the U.S. Government.				
17. COSATI CODES			18. SUBJECT TERMS (continue on reverse if necessary and identify by block number)	
FIELD	GROUP	SUBGROUP	Thermal Imaging Systems, FLIR Performance	
19. ABSTRACT (continue on reverse if necessary and identify by block number) The minimum resolvable temperature difference (MRTD) is widely accepted as the parameter that best describes the field performance of a thermal imaging system (TIS). Mathematical modeling that accurately predicts the MRTD has been of major interest to the infrared community over the last 30 years. This work reviews the currently accepted models for predicting the MRTD. Simplifying assumptions used by these models which deal with the target spectrum are discussed and tested using specifications taken from a standard forward looking infrared (FLIR) system. In addition new models are proposed and tested. Two of these models are a direct extension of the recently proposed Vortman-Bar-Lev adaptive matched filter. A third model is based on the novel concept that the MRTD curve is predictable from a threshold condition on the visibility rather than the signal-to-noise ratio, of the system-degraded bar pattern.				
20. DISTRIBUTION/AVAILABILITY OF ABSTRACT <input checked="" type="checkbox"/> UNCLASSIFIED/UNLIMITED <input type="checkbox"/> SAME AS REPORT <input type="checkbox"/> DTIC USERS			21. ABSTRACT SECURITY CLASSIFICATION Unclassified	
22a. NAME OF RESPONSIBLE INDIVIDUAL Pieper, R. J.			22b. TELEPHONE (Include Area code) 408-646-2101	22c. OFFICE SYMBOL EC/Pr

Approved for public release; distribution is unlimited.

MODELING FOR IMPROVED  
MINIMUM RESOLVABLE TEMPERATURE DIFFERENCE  
MEASUREMENTS

by

Alejandro R. Ugarte  
Lieutenant, Argentine Navy  
Escuela Naval Militar, Argentina, 1980

Submitted in partial fulfillment  
of the requirements for the degree of

MASTER OF SCIENCE IN ELECTRICAL ENGINEERING  
MASTER OF SCIENCE IN SYSTEMS ENGINEERING  
(ELECTRONIC WARFARE)

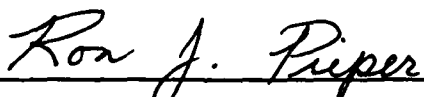
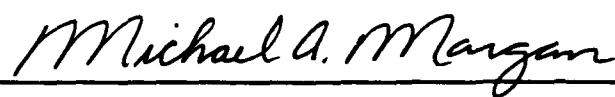

from

NAVAL POSTGRADUATE SCHOOL  
September 1991

Author:

  
Alejandro R. Ugarte

Approved by:

  
Ron J. Pieper, Thesis Advisor  
John P. Powers, Second Reader  
Michael A. Morgan, Chairman,  
Department of Electrical & Computer Engineering  
Joseph Sternberg, Chairman,  
Electronic Warfare Academic Group

## ABSTRACT

The minimum resolvable temperature difference (MRTD) is widely accepted as the parameter that best describes the field performance of a thermal imaging system (TIS). Mathematical modeling that accurately predicts the MRTD has been of major interest to the infrared community over the last 30 years. This work reviews the currently accepted models for predicting the MRTD. Simplifying assumptions used by these models which deal with the target spectrum are discussed and tested using specifications taken from a standard forward looking infrared (FLIR) system. In addition new models are proposed and tested. Two of these models are a direct extension of the recently proposed Vortman-Bar-Lev adaptive matched filter. A third model is based on the novel concept that the MRTD curve is predictable from a threshold condition on the visibility, rather than the signal-to-noise ratio, of the system-degraded bar pattern.



Accession For	
NTIS GRA&I	<input checked="checked" type="checkbox"/>
DTIC TAB	<input type="checkbox"/>
Unannounced	<input type="checkbox"/>
Justification	
By	
Distribution/	
Availability Codes	
Dist	Avail and/or Special
A-1	

## TABLE OF CONTENTS

I. INTRODUCTION . . . . .	1
A. REVIEW OF LITERATURE . . . . .	1
B. OVERVIEW OF THE THESIS . . . . .	2
C. FUNDAMENTALS OF THERMAL IMAGING SYSTEMS . . .	3
D. BASIC PARAMETERS . . . . .	5
E. MINIMUM RESOLVABLE TEMPERATURE DIFFERENCE (MRTD) . . . . .	9
F. NECESSITY OF A MODEL . . . . .	10
G. MOTIVATION FOR THIS WORK . . . . .	12
II. ESTABLISHED MRTD MODELS . . . . .	16
A. SYSTEM DESCRIPTION . . . . .	16
1. NETD Calculation for the Sample System . . .	17
B. THE RATCHES MODEL FOR THE SAMPLE SYSTEM . . . .	20
C. THE LLOYD APPROXIMATE MODEL FOR THE SAMPLE SYSTEM . . . . .	22
D. THE VORTMAN AND BAR-LEV MODEL FOR THE SAMPLE SYS- TEM . . . . .	25
III. PROPOSED MRTD MODELS . . . . .	30
A. MODIFIED VORTMAN AND BAR-LEV MODEL FOR THE SAMPLE SYSTEM . . . . .	30

B. A VISIBILITY MODEL FOR MRTD MEASUREMENTS . . .	33
C. INCLUSION OF SAMPLING ARTIFACTS. EFFECTS ON THE RATCHES MODEL . . . . .	41
IV. COMPARATIVE ANALYSIS AND CONCLUSIONS . . . . .	47
APPENDIX A - INTERPRETATION OF THE RATCHES MODEL . .	50
A. PRELIMINARIES . . . . .	51
B. DERIVATION OF THE NOISE EQUIVALENT TEMPERATURE DIFFERENCE (NETD) . . . . .	54
C. DERIVATION OF THE MINIMUM RESOLVABLE TEMPERATURE DIFFERENCE (MRTD) . . . . .	65
APPENDIX B - DESCRIPTIVE FLOWCHARTS OF SIMULATION . . .	79
APPENDIX C - EXACT FOUR-BAR FOURIER SPECTRUM . . . . .	80
APPENDIX D - SAMPLE SYSTEM . . . . .	87
LIST OF REFERENCES . . . . .	89
INITIAL DISTRIBUTION LIST . . . . .	93

## TABLE OF SYMBOLS

$\alpha$ :	Modified visibility parameter
$\beta$ :	Parameter to express $\Delta T_{sc}$ as a function of NETD
$\Gamma$ :	Constant to convert units of noise [ $^{\circ}\text{C}^2$ mrad]
$\Delta\phi_{(\lambda)}$ :	Wavelength dependent part of $P_{(\lambda,t)}$ [watts/ $\mu\text{m}$ ]
$\Delta f_n$ :	Noise equivalent electrical bandwidth [Hz]
$\Delta f_{xn}$ :	Noise equivalent electrical bandwidth [cy/mrad]
$\Delta T$ :	Target-background temperature difference [ $^{\circ}\text{C}$ ]
$\Delta T_s$ :	Apparent temperature difference (Mod. Visib.) [ $^{\circ}\text{C}$ ]
$\Delta T_{sc}$ :	Threshold $\Delta T_s$ for resolution (Mod. Visib.) [ $^{\circ}\text{C}$ ]
$\Delta x$ :	Horizontal DAS [mrad]
$\Delta y$ :	Vertical DAS [mrad]
$\Delta y_i$ :	Angular distance between scan lines ( $\Delta y/\eta_{ovsc}$ ) [mrad]
$\eta_{o(\lambda)}$ :	Optical efficiency of the viewer
$\eta_{ovsc}$ :	Overscan Ratio for the device
$\eta_{sc}$ :	Scan efficiency
$\lambda$ :	Wavelength of monochromatic infrared radiation [ $\mu\text{m}$ ]
$\lambda_p$ :	Characteristic wavelength of the detectors [ $\mu\text{m}$ ]
$\sigma$ :	Root mean square noise at the output of $H_{ELECT}$ [volts]
$\Psi$ :	Threshold signal-to-noise ratio for resolution
$a$ :	CRT spot size parameter
$A$ :	Normalized spatial frequency for optics MTF [Hz]
$A_d$ :	Area of a single detector [ $\text{cm}^2$ ]

$A_t$ : Total Area of the target [ $\text{mrad}^2$ ]  
 $b_{i(x)}$ : Noise along the  $i^{\text{th}}$  video line  
 $d$ : Focal length of collecting lens [cm]  
 $D$ : Diameter of collecting lens [cm]  
 $D_{(\lambda)}^*$ : Specific detectivity as a function of wavelength  
 [cm(Hz) $^{.5}$ /watt]  
 DAS: Detector Angular Subtense [mrad]  
 $F$ :  $F/\text{Number} = d/D$   
 FLIR: Forward Looking InfraRed  
 $f_{ox}$ : Horizontal spatial frequency of the target [cy/mrad]  
 $f_r$ : 3-dB frequency of electronic Roll-Off [Hz]  
 $F_r$ : Frame rate [Hz]  
 $f_{rx}$ : 3-dB frequency of electronic Roll-Off [cy/mrad]  
 $f_x$ : Spatial frequency along the horizontal direction  
 [cy/mrad]  
 $f_y$ : Spatial frequency along the vertical direction  
 [cy/mrad]  
 $H_{(\lambda)}$ : Spectral irradiance onto a detector [watt/( $\text{cm}^2 \cdot \mu\text{m}$ )]  
 $H_d$ : Display MTF  
 $H_o$ : Overall System MTF ( $H_{opt}H_{det}H_{ELECT}H_d$ )  
 $H_{det}$ : Detector MTF  
 $h_{\text{DET-ELECT}}$ : Detector-electronics impulse response [volts/watt]  
 $h_{\text{ELECT}}$ : Electronics impulse response  
 $H_{\text{ELECT}}$ : Electronics MTF  
 HFOV: Horizontal Field of View [mrad]  
 $H_{mf}$ : Matched Filter MTF



$H_{opt}$ : Optics MTF  
 $H_T$ : Normalized Fourier transform of the target  
 $H_u$ : Normalized Fourier transform of one bar (along x)  
 $i_{(t)}$ : Normalized time dependent part of  $P_{(\lambda,t)}$   
 $i'_{(t)}$ :  $i_{(t)} \star r_{(t)} \star h_{ELECT(t)}$   
 $i_{(x,y)}$ : Spatial description of the displayed target  
 $i_T(x,y)$ : Spatial description of the actual target  
 $I_T$ : Fourier Transform of the target  
 $k$ : constant to transform temperature into radiant  
     displayed energy [watt/°C]  
 $K$ : Constant to define a Matched Filter  
 $L$ : Length of the bars of the standard target [mrad]  
 $L_{(\lambda)}$ : Spectral Radiance from source [watts/(cm<sup>2</sup> sr  $\mu$ m)]  
 $M_{(x,y)}$ : Signal energy per unit area of display [Joule/mrad<sup>2</sup>]  
 $MRTD$ : Minimum Resolvable Temperature Difference [°C]  
 $MTF$ : Modulation Transfer Function (all are normalized)  
 $n_{(x,y)}$ : Spatial description of displayed noise [Joule/mrad<sup>2</sup>]  
 $NEP_{(\lambda)}$ : Spectral Noise Equivalent Power [watts]  
 $NETD$ : Noise Equivalent Temperature Difference [°C]  
 $NETD'$ : NETD converted into radiant displayed energy [Joule]  
 $n_p$ : Number of detectors in parallel  
 $P_{(\lambda,t)}$ : Time-varying spectral radiant flux on a detector  
     [watts/ $\mu$ m]  
 $PSD$ : Power Spectral Density [Watts/Hz]  
 $r$ : Detector response function [volts/watt]  
 $R$ : Autocorrelation function

$R_{(\lambda)}$ : Wavelength dependent part of the Fourier transform  
of  $r$   
 $R_{(f)}$ : Frequency dependent part of the Fourier transform of  
 $r$   
 $t_e$ : Eye integration time [sec]  
 $S'_i$ : Single-sided Noise PSD at system input [Watts/freq]  
 $S'_o$ : Single-sided Noise PSD at system output [Watts/freq]  
 $S_i$ : Double-sided Noise PSD at system input [Watts/freq]  
 $S_o$ : Double-sided Noise PSD at system output [Watts/freq]  
 $t$ : time [sec]  
 $T$ : Temperature [ $^{\circ}\text{C}$ ]  
 $T_b$ : Background Temperature [ $^{\circ}\text{C}$ ]  
TIS: Thermal Imaging System  
VFOV: Vertical Field of View [mrad]  
 $V_n$ : Noise Voltage at the output of  $H_{\text{ELECT}}$   
 $V_s$ : Signal Voltage at the output of  $H_{\text{ELECT}}$   
 $V_{s(t)}$ : Instantaneous output voltage from detector-electron-  
ics [volts]  
 $\tau_d$ : Detector dwelltime [sec]  
 $v_x$ : Horizontal scanning velocity [mrad/sec]  
 $W$ : Width of a single bar of the standard target [mrad]  
 $y_i$ : Vertical coordinate of the  $i^{\text{th}}$  video line [mrad]

## ACKNOWLEDGEMENTS

I would like to thank Professor Ron J. Pieper for his continuous guidance in the pursuit of this thesis. It is also my sincere duty to acknowledge my EW Curricular Officer and his staff for their support.

I would like to thank the Argentine Navy and the U.S. Navy for providing this opportunity.

Lastly I would like to express my sincere thanks to my wife, Martha, for her support and patience during my stay here.

## I. INTRODUCTION

### A. REVIEW OF LITERATURE

The minimum resolvable temperature difference (MRTD) has been widely accepted as the parameter that best describes the field performance of a thermal imaging system (TIS) when involved in recognition and identification tasks [Ref. 1], [Ref. 2], [Ref. 3], [Ref. 4].

It became a popular design tool for forward looking infrared (FLIR) systems in 1975, when the U.S. Army Night Vision Laboratory (NVL) published a successful mathematical model [Ref. 5] which was based on matched filter theory as an alternative to the predated perfect synchronous integrator model [Ref. 6]. In spite of its success, shortcomings have been encountered in both mathematical modelling, and measurement of the MRTD for TIS [Ref. 7], [Ref. 8].

To improve the MRTD prediction, other models have been proposed, by either modifying the original from Ratches [Ref. 8], including particular concepts for specific types of systems, or using generic expressions valid for any type of TIS [Ref. 9].

Perhaps the most critical issues in MRTD modelling are:

1. **visual perception**, which has been an area of fundamental research by several authors such as Johnson, Blackwell, Schade, Genoud, Sendall, Rose [Ref. 10], Rosell, Willson

[Ref. 11], Kornfeld and Lawson [Ref. 12], [Ref.13], [Ref. 14], [Ref. 15], [Ref.16].

2. **effects of sampling**, [Ref. 17], [Ref. 18], [Ref. 19], [Ref. 20], [Ref. 21].

3. **noise characteristics**, [Ref. 5], [Ref. 8], [Ref. 2].

With respect to MRTD measurements, **objectivity** has been the main goal. Several laboratories are currently offering high quality MRTD measurements following procedures that, though very similar in principles, slightly vary according to special needs. The use of computers and voltage prior to the display to eliminate the logical operators' subjectivity is being experimented using not only vertical targets but also rotated ones for paarticular applications [Ref. 1], [Ref. 2], [Ref. 23], [Ref. 24], [Ref. 25], [Ref. 26].

## **B. OVERVIEW OF THE THESIS**

The present chapter introduces the fundamentals of the MRTD as a figure of merit for a TIS and the discrepancies currently reported between predicted and measured data.

Chapter II briefly describes MRTD models from Ratches [Ref. 5], Lloyd [Ref. 10, p. 184], and Vortman and Bar-Lev [Ref. 8] that apply matched filter theory and presents their predictions for the sample system given in Appendix D.

Chapter III considers four proposed models: the first two modify the matched filter presented by Vortman and Bar-Lev, the third uses the concept of visibility of the system-degra-

ded bar pattern, and the fourth shows the effects of sampling artifacts on the original Ratches model.

In Chapter IV a comparative analysis between the different models is performed, their feasibility analyzed, and the final conclusions stated.

Appendix A covers the development of Ratches model, Appendix B presents a flowchart to provide a pedagogical description of the simulations performed in MATLAB, Appendix C includes the spectral analysis of the standard MRTD target, and Appendix D lists the data of the sample system used for the different simulations.

For typographical convenience a non-conventional notation has been adopted for all the equations in this work. Specifically, the functional dependence is shown as a subscripted argument leading to a more compact form, i.e.,  $h_i(x,y)$  is represented as  $h_{i(x,y)}$ .

### C. FUNDAMENTALS OF THERMAL IMAGING SYSTEMS

An object that presents an apparent temperature difference with respect to the background can be detected, and subsequently recognized and identified by means of a thermal imaging system. This difference in apparent temperature has to be large enough to overcome variations in the background temperature and other sources of noise, as well as the eventual attenuation produced by the atmosphere along the energy path. The term **apparent** describes the fact that different

emissivities may need to be considered for target and background.

Due to their popularity and simplicity, only conventional scanning thermal imaging systems, known as FLIRs, will be considered within the scope of this work. Consideration of other recent designs, e.g., mosaic staring infrared systems, infrared linescanners, or pyroelectric array systems that present particular characteristics, would require an extension of this investigation beyond the limitation in time imposed. This section follows the description presented by Lloyd [Ref. 10, p. 15], whose text has been accepted as a fundamental reference by the entire infrared community. Figure I.1 shows one possible way of implementing a FLIR.

The optical system collects, spectrally filters, spatially filters, and focusses the radiation pattern from the scene onto a focal plane containing a single small element. An opto-mechanical scanner consisting of a set of two scanning mirrors, one sweeping vertically and the other horizontally, is interposed between the optical system and the detector. The ray bundle reaching the detector from the object moves as the mirrors move, tracing out a TV-like raster in object space as shown in Figure I.1. This process of detecting the scene sequentially is called scene dissection [Ref. 10, p. 8].

The energy of the electromagnetic field incident onto the detector produces a response in the form of an electronic signal that is then processed by amplification and filtering circuits.

Finally, the TIS requires a display in synchronism with the scanning components, such that the image is presented to the observer in an appropriate way.

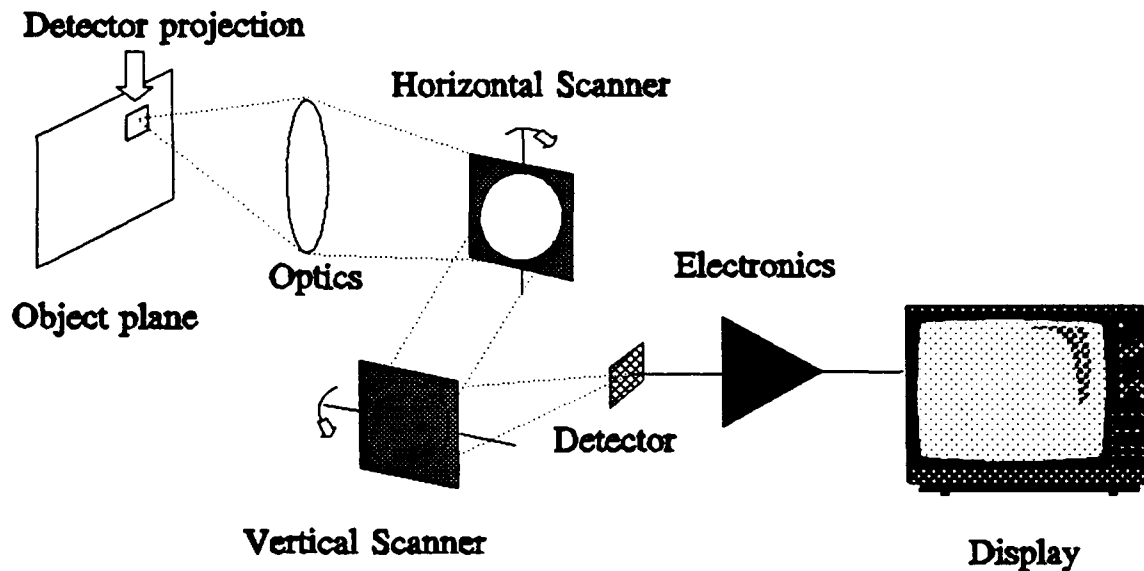


Figure I.1. Simplified FLIR (After Ref. 10, p. 10)

The system can be represented by a block diagram of four basic cascaded components, which filter the incoming electromagnetic signal: optics, detector, electronics, and display. Figure I.2 depicts this concept and introduces the symbology of the individual transfer functions.

#### D. BASIC PARAMETERS

A system with such a diversity of components as a TIS has a great number of parameters that describe the particular performance of each element. Braddick and Ludlow [Ref. 1] list more than twenty different parameters of importance in



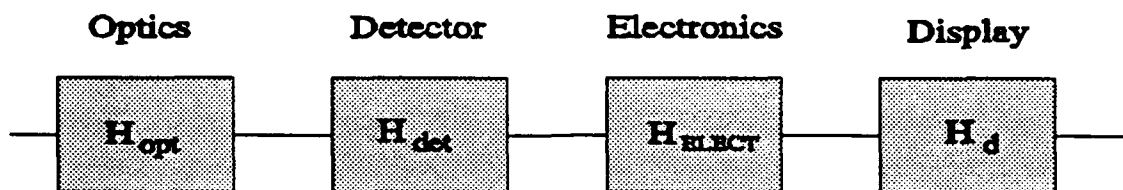


Figure I.2. Block Diagram of Simplified FLIR

TIS design and evaluation. However, finding a single parameter to describe the overall performance of a system has always been of primary interest for engineers.

From the beginning, the infrared community identified two basic aspects of fundamental importance in TIS assessment: thermal resolution and spatial resolution. Historically, they lead to the first two parameters of common use: the Noise Equivalent Temperature Difference (NETD) and the Detector Angular Subtense (DAS). The former is related to thermal resolution; the latter, to spatial resolution.

The NETD can be considered as "a measure of the ability of a system to discriminate small signals in noise" although a more proper definition follows: "the NETD is the blackbody target-to-background temperature difference in a standard test pattern which produces a peak-signal to rms-noise ratio (SNR) of one at the output of a reference electronic filter when the system views the test pattern". [Ref. 10, p. 166]

If the temperature difference between target and background is denoted by  $\Delta T$  (the target must be at a higher temperature than the background), the signal voltage by  $V_s$  and the rms noise voltage by  $V_n$ , the NETD can be obtained from:

$$\text{NETD} = \frac{\Delta T \cdot V_n}{V_s} . \quad (\text{I.1})$$

It follows that, if the signal voltage equals the noise voltage, the NETD is the temperature difference between target and background. Figure I.3 shows the general appearance of the target-background arrange as well as a typical voltage waveform for a scanned line. The observed DC droop is an unwanted signal degradation due to the time constant of the dc-blocking circuitry employed to couple the detector and the required amplifying electronics and can be minimized [Ref. 10, pp. 336-345].

Equation (I.1) is a basic expression that describes the concept of the NETD as a figure of merit. Appendix A provides a detailed explanation of the measurement process and a mathematical model for the NETD.

On the other hand, the more intuitive concept of DAS can be defined as the angle subtended by the projection of the limits of a detector on the object plane. It is customary to denote the horizontal DAS by  $\Delta x$ , and the vertical DAS by  $\Delta y$ . The time required to scan through an horizontal angular subtense is known as dwelltime. Figure I.4 shows a magnified

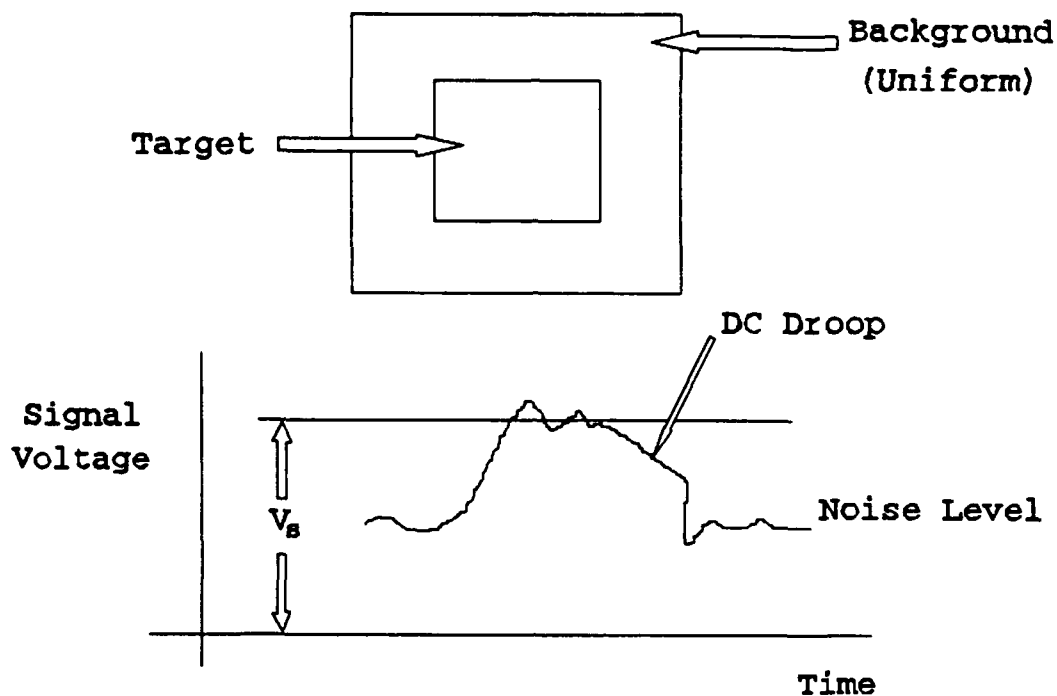


Figure I.3. NETD target and voltage waveform  
(After Ref. 10, p. 167)

projection of the DAS on the object plane, as well as the horizontal (HFOV) and vertical (VFOV) fields of view.

But this information is not descriptive enough. Thermal Imagers have been mainly used to recognize and identify "targets". Therefore, it is reasonable to look for a parameter that describes their overall performance in those terms. As it is discussed in Appendix A, the NETD and DAS are employed in the determination of a more elaborate and appropriate parameter: The Minimum Resolvable Temperature Difference (MRTD).

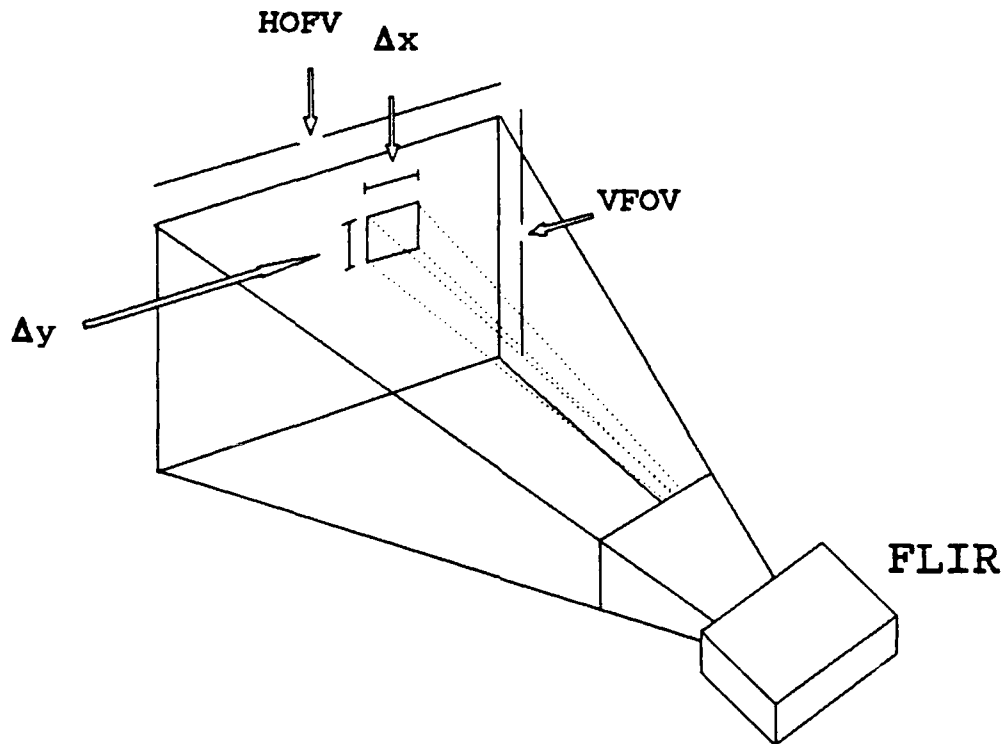


Figure I.4. Detector Angular Subtense (DAS) (After Ref. 10)

#### E. MINIMUM RESOLVABLE TEMPERATURE DIFFERENCE (MRTD)

The results obtained by Schade [Ref. 10, p. 183] for resolution in photographic, motion picture, and television systems were adapted by Genoud and Sendall [Ref. 10, p. 183] to infrared systems.

Infrared imaging systems are commonly involved in recognition and identification of military ground vehicles. It was shown [Ref. 27] that the probability of recognizing and identifying a main battle tank is related to the ability of the system to resolve bar targets in a laboratory experiment.

The infrared community has selected the MRTD test to be the industry standard for characterizing the performance of a thermal imaging system. The standard pattern was chosen to be consisting of four vertical bars of 7:1 aspect ratio (the bar height is seven times the bar width) on a background of uniform temperature. The bar centers are separated by twice the width of the bars. Currently, most MRTD measurements are performed using this target.

The difference in apparent temperature between the target and the background is controlled until the pattern becomes recognizable. (If human observers are employed, majority of opinions is required to accept that the target was recognized.) That temperature difference which brings the signal above the noise and makes the four bars visible is the value of MRTD for the particular spatial frequency of the target. Figure I.5 shows a sample set of four targets of different spatial frequencies. It is noted that as the spatial frequency increases, the overall target size decreases.

#### **F. NECESSITY OF A MODEL**

The need for a mathematical model to represent the MRTD is quite obvious since it is the best tool a designer can count on to forecast the task performance of a future infrared imaging system. Unfortunately, in the process of recognition and identification, the ability of the observer's eye and brain to handle the image presented on the display is of

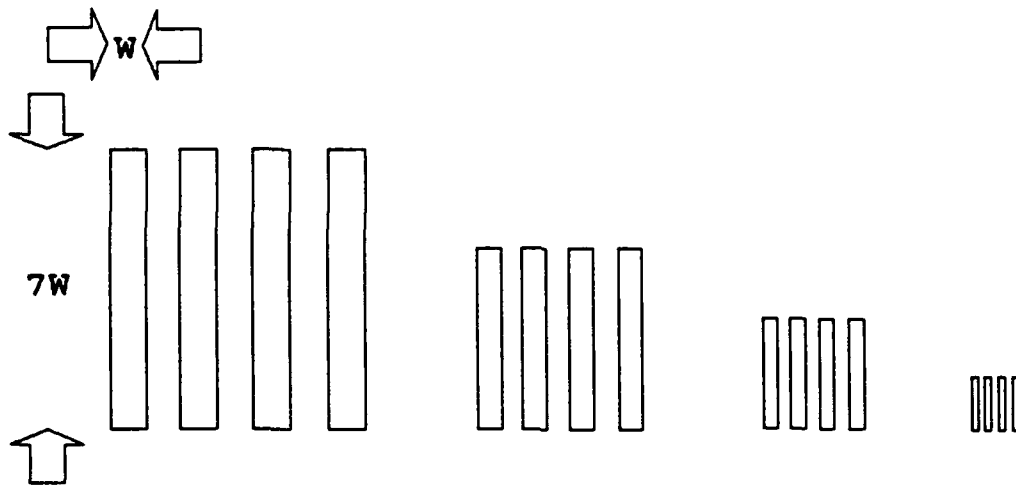


Figure I.5. Sample four different spatial frequency targets

fundamental importance, and then the model must include a complex [Ref. 13] and not completely understood [Ref. 7] process involving eye and brain.

The Ratches model [Ref. 5] defines the MRTD in terms of a scanning system's elemental parameters and represents the human eye-brain system by a matched filter. It is extensively treated in Appendix A and is the basis of this work. A typical predicted MRTD curve, corresponding to the sample system (Appendix D) that is employed in this investigation, is shown in Figure I.6 (approximated).

### Predicted MRTD (Sample FLIR)

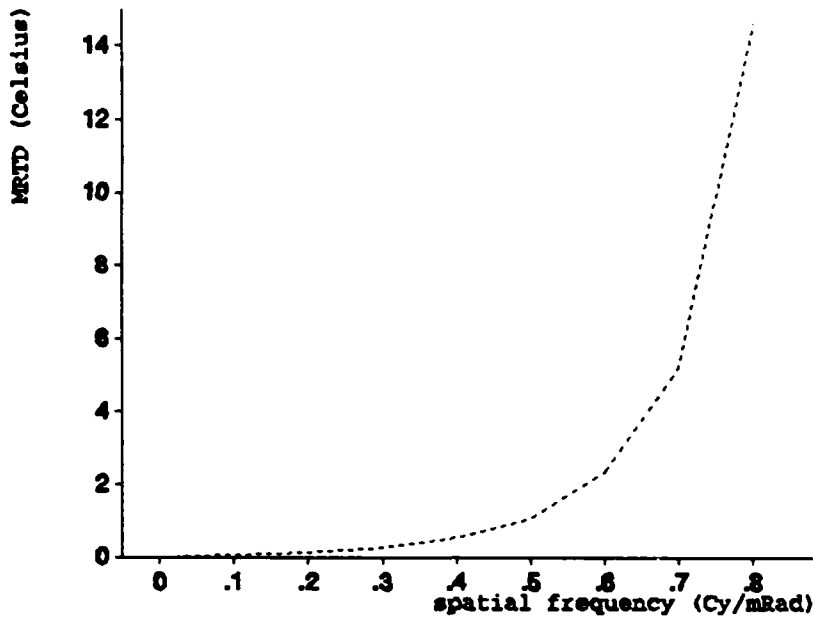


Figure I.6. Sample MRTD curve

#### G. MOTIVATION FOR THIS WORK

In spite of the success of the Ratches model, there still is discrepancy between predicted and measured data. Several authors have reported underestimation of the MRTD in the low spatial frequencies (too optimistic prediction) as well as differences in the high spatial frequencies. Figures I.7 to I.10 clearly show this situation as presented by three different authors for four typical systems. Figures I.7 and I.8, from Vortman and Bar-Lev [Ref. 8], include, besides the Ratches model (represented by RL) and measured data, two other models: LSI, not discussed in this thesis, and AMF, presented

in Chapter II. Both frequency and temperature are normalized with respect to unknown (to this author) constants  $f_r$  and  $K_{1,2}$ , respectively. In both figures a general optimistic behavior of the Ratches model is observed. Figure I.9 from Braddick and Ludlow [Ref. 1] shows a calculated MRTD based on a different, though similar, model [Ref. 24], and Figure I.10 from McCracken and Wajsfelner [Ref. 7] plots predictions from the Ratches model. These two figures show a mixed behavior of the Ratches model: too optimistic in the low spatial frequencies and too optimistic in the high spatial frequencies when compared with measured data.

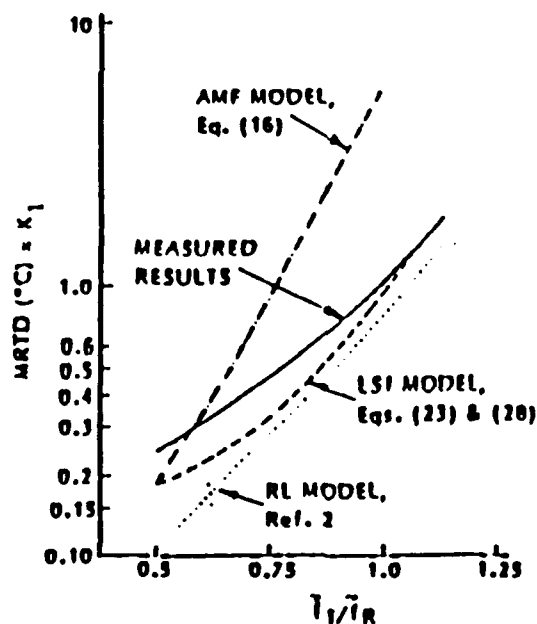


Figure I.7. MRTD vs. Spatial Frequency  
(from Ref. 8)



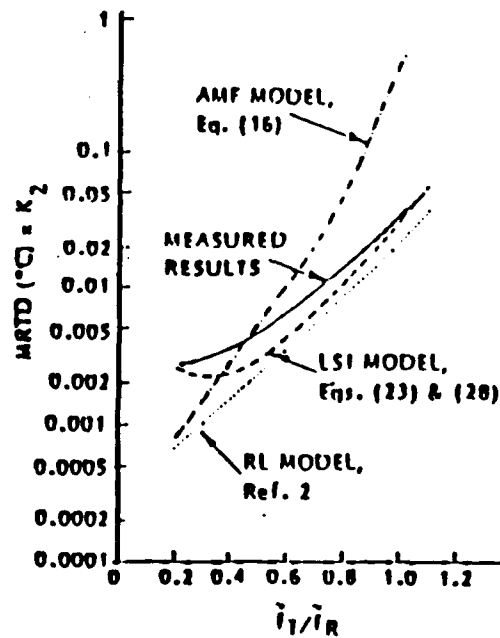


Figure I.8. MRTD vs. Spatial Frequency  
(from Ref. 8)

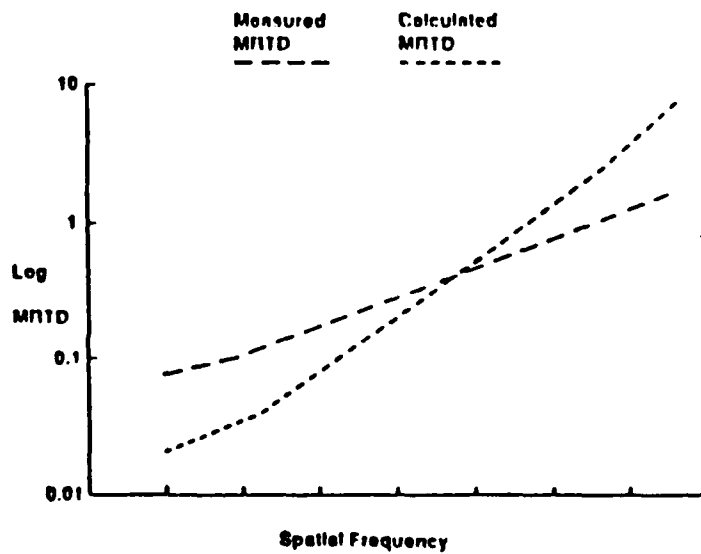


Figure I.9. MRTD vs. Spatial Frequency  
(from Ref. 1)

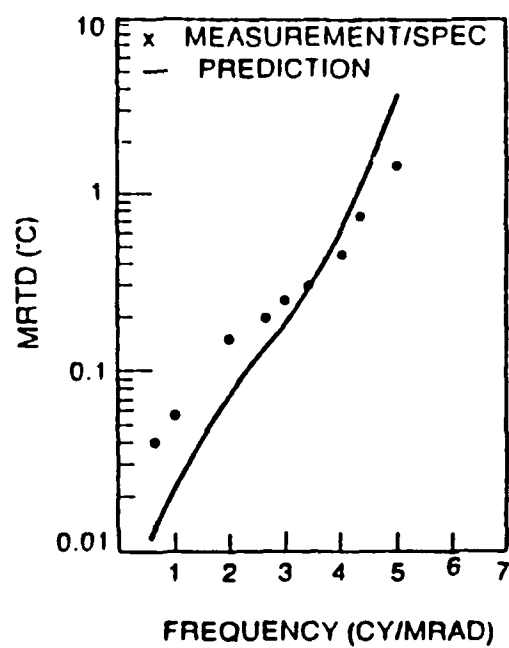


Figure I.10. MRTD vs. Spatial Frequency  
(from Ref. 10)

## II. ESTABLISHED MRTD MODELS

### A. SYSTEM DESCRIPTION

Only the effects of the four cascaded transfer functions presented in Figure I.2 have been considered to obtain the overall transfer function of the system. Expressed in horizontal spatial frequency domain ( $f_x$ ), these are [Ref. 28]:

1. Optical diffraction limit ( $H_{opt}$ ):

$$H_{opt}(f_x) = \frac{2}{\pi} \{ \cos^{-1}(A) - A\sqrt{1-A^2} \} \quad (II.1)$$

where  $A = (\lambda F f_x / d) 1000$ ,  $F$  is the f/number and  $d$  is the focal length using the units defined in Appendix D. This strictly positive function is nonzero over the range of the normalized spatial frequency,  $A$ , equal to  $[0,1]$ . It is derived from the autocorrelation of the pupil function of a spherical lens for an incoherent optical system. [Ref. 10, pp. 99-103]

2. Detector spatial filter ( $H_{det}$ ):

$$H_{det}(f_x) = \frac{\sin(\pi f_x \Delta x)}{(\pi f_x \Delta x)} \quad (II.2)$$

where  $\Delta x$  is the detector angular subtense (x direction).

3. Electronics ( $H_{ELECT}$ ):

$$H_{ELECT}(f_x) = \frac{1}{\sqrt{1 + \left( \frac{f_x}{f_{rx}} \right)^2}} \quad (II.3)$$

The MTF  $H_{ELECT}$  is more commonly expressed as a function of temporal frequency. The conversion from temporal to spatial frequency can be performed by the relation:

$$f_x = \frac{f}{v_x} \quad (\text{II.5})$$

where  $f_x$  is the spatial frequency,  $f$  is the temporal frequency and  $v_x$  is the horizontal angular scanning velocity [mrad/sec]. [Ref. 5], [Ref. 9], [Ref. 28]

#### 4. CRT display or monitor ( $H_d$ )

$$H_d(f_x) = e^{(-\pi f_x^2)} \quad (\text{II.4})$$

This is equivalent to assuming that the display can be described by an incoherent point spread function with a gaussian space dependence [Ref. 29].

Figure II.1 shows the four individual modulation transfer functions and Figure II.2 shows the overall modulation transfer function of the system.

#### 1. NETD Calculation for the Sample System

The complete derivation of the NETD and MRTD models presented by the Night Vision Laboratory are included in Appendix A, where the NETD expression is repeated here for reader convenience (A.32):

$$\text{NETD} = \frac{4F^2 (\Delta f_n)^{\frac{1}{2}}}{\pi A_d^{\frac{1}{2}} \int_0^\infty \eta_{0(\lambda)} \frac{\partial L_{(\lambda)}}{\partial T} D_{(\lambda)}^* d\lambda} \quad (\text{II.6})$$

Several standard approximations are applied to (II.6) in order to facilitate the NETD calculation. By linearizing the specific detectivity ( $D_{(\lambda)}^* = \lambda D_{(\lambda_p)}^* / \lambda_p$ ), and considering the

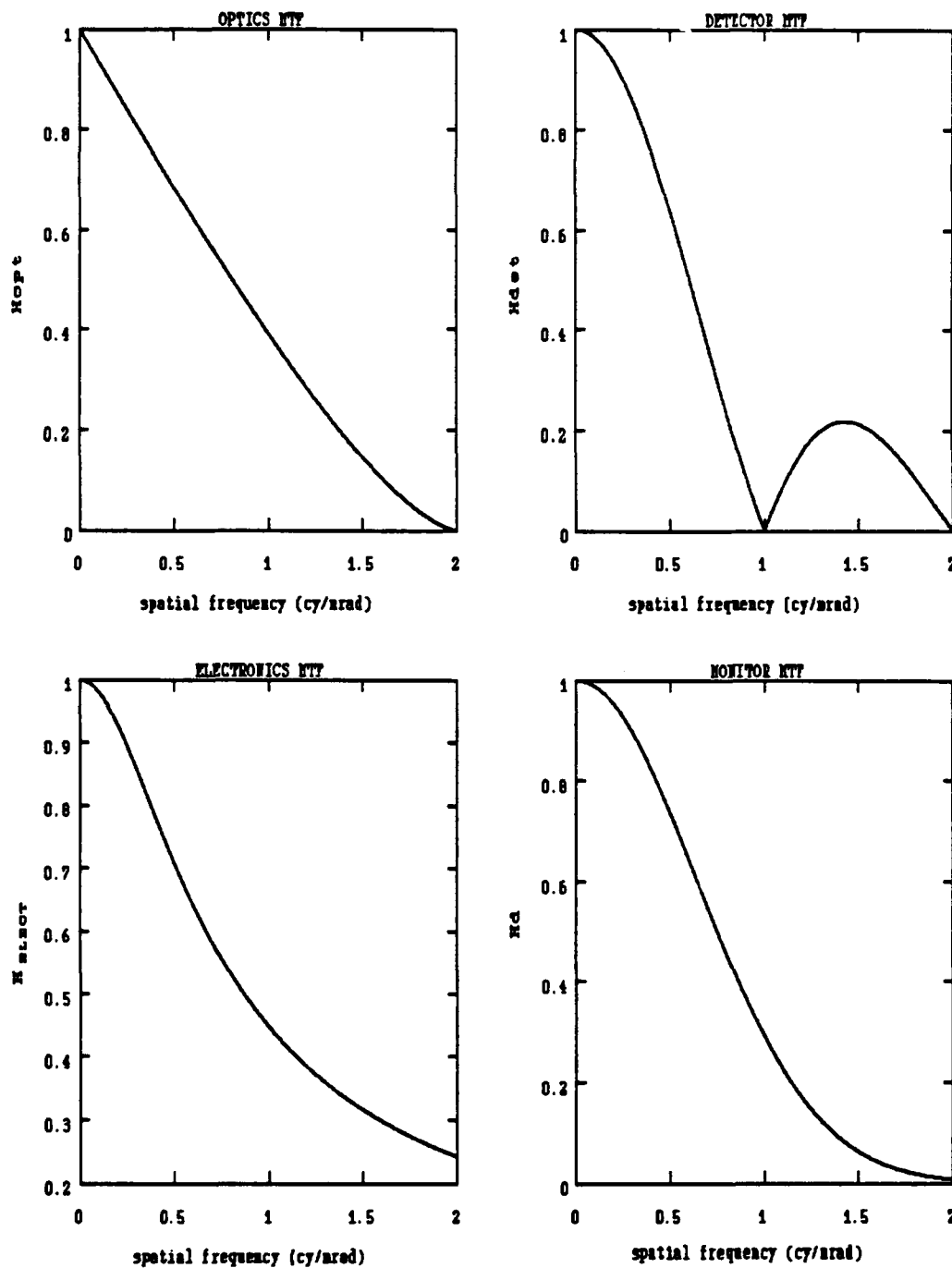


Figure II.1. Individual MTFs of the sample system

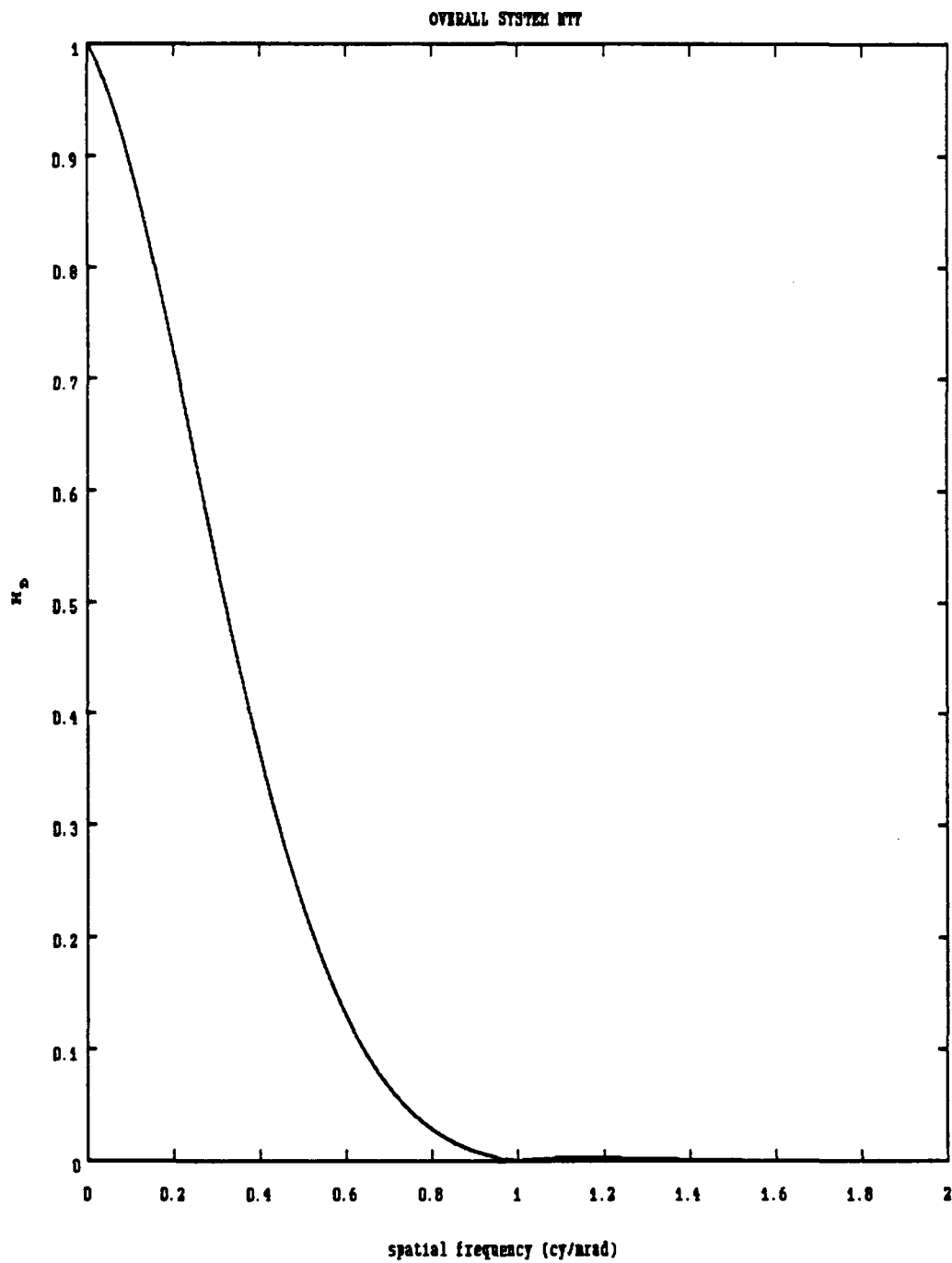


Figure II.2: Overall MTF of the sample system

actual spectral bandpass of the system (8-11.5  $\mu\text{m}$ ), the integral in (II.6) can be replaced by:

$$\eta_{o(\lambda_p)} D_{(\lambda_p)}^* \int_8^{11.5} \frac{\partial L_{(\lambda)}}{\partial T} \frac{\lambda}{\lambda_p} d\lambda \quad (\text{II.7.a})$$

Employing the approximation from Lloyd [Ref. 10, p. 174], based on the radiation slide rule,

$$\left. \frac{\partial L_{(\lambda, T)}}{\partial T} \right|_{T_B} = \frac{c_2}{\lambda T_B^2} L_{(\lambda, T_B)} \quad (\text{II.7.b})$$

where  $c_2 = 1.4388 \times 10^4$  [ $\mu\text{m} \cdot ^\circ\text{C}$ ] and  $T_B$  is the background temperature. The evaluation of the integral in (II.7.a), for the sample system yields  $4.71 \times 10^{-5}$  [watt/( $\text{cm}^2 \text{ st} \cdot ^\circ\text{C}$ )] and the approximate NETD (II.6) is then evaluated using specified values taken from Appendix D:

NETD

$$= \frac{4 (2.5)^2 \sqrt{29400 \text{ [Hz]}}}{\pi [\text{st}] (0.005 [\text{cm}]) (0.8) (2 \times 10^{10} [\frac{\text{cm Hz}^{1/2}}{\text{watt}}]) (4.71 \times 10^{-5} [\frac{\text{watt}}{\text{cm}^2 \text{ st} \cdot ^\circ\text{C}}])}$$

$\approx 0.36^\circ\text{C}$

## B. THE RATCHES MODEL FOR THE SAMPLE SYSTEM

As derived in Appendix A (A.62), the complete expression for the MRTD using the Ratches Model is:

MRTD

$$\begin{aligned}
 &= \frac{\frac{\pi^2}{8} \Psi \text{ NETD}}{H_D(f_{ox}) L \int_{-\infty}^{\infty} H_T^2(f_y) H_D^2(f_y) df_y} \\
 &\cdot \left[ \frac{v_x \Delta y_i}{\Delta f_n F_r t_e} \int_{-\infty}^{\infty} \int_0^{\infty} \frac{S'_i(f_x)}{S'_i(f_{rx})} H_{\text{ELECT}}^2(f_x) H_d^2(f_x, f_y) H_w^2(f_x) H_T^2(f_y) H_D^2(f_y) df_x df_y \right]^{\frac{1}{2}}.
 \end{aligned} \tag{II.8}$$

To obtain this equation Ratches et al. performed the following basic steps:

1. The actual target consisting of four vertical bars is assumed to be periodic in the horizontal direction.
2. The human eye-brain system is represented by a matched filter consisting of one bar undegraded in the horizontal direction and degraded in the vertical direction, i.e.,

$$H_{mf}(f_x, f_y) = H_{T1bar}(f_x, f_y) H_D(f_y) = H_w(f_x) H_T(f_y) H_D(f_y) \tag{II.9}$$

3. The signal is obtained by taking the difference between the output of that matched filter when centered over the displayed bars and when centered over the background. The signal is referred to temperature units.
4. The noise in the display is assumed to be white and it is referred to temperature units by means of the NETD and the noise equivalent electrical bandwidth  $\Delta f_n$ .
5. The signal-to-noise ratio present at the display is improved by two factors related to the operator: the eye-brain matched filter and the integration performed by the eye over one eye integration time.
6. Resolution of the bars is considered to be achieved when the signal-to noise ratio has exceeded a threshold value  $\Psi$ . In the case of Ratches' paper, the experimental value recommended for  $\Psi$  is 2.25 [Ref. 5], [Ref. 8]. However, Lloyd recommends a different value based on probability of detection of single bars of 90 percent:  $\Psi=4.5$  [Ref. 10, p. 188]. Since this difference does not affect the shape of the general curve, and in order to be consistent with the plot presented by the latter, the



simulation of the Ratches model is performed with the second threshold value of signal-to-noise ratio.

The computer simulation of (II.8) for the sample system provides the plots shown in Figure II.3 (linear and logarithmic scales). MRTDs are commonly expressed in Celsius degrees [Ref. 5].

### C. THE LLOYD APPROXIMATE MODEL FOR THE SAMPLE SYSTEM

The authors of the Night Vision Laboratory model [Ref. 5], present some approximations to (II.8) to allow hand calculations. These approximations -acceptable only for low spatial frequencies- are:

$$L \int_{-\infty}^{\infty} H_{T(f_y)}^2 H_{D(f_y)}^2 H_{d(f_y)}^2 df_y = 1, \quad (\text{II.10.a})$$

$$L \int_{-\infty}^{\infty} H_{T(f_y)}^2 H_{D(f_y)}^2 df_y = 1, \text{ and} \quad (\text{II.10.b})$$

$$2W \int_0^{\infty} \frac{S'_{i(f_x)}}{S'_{i(f_{rx})}} H_{\text{ELECT}(f_x)}^2 H_{d(f_x)}^2 H_{w(f_x)}^2 df_x = 1, \quad (\text{II.10.c})$$

since from definitions of  $H_{w(f_x)}$  and  $H_{T(f_y)}$  given in Appendix C:

$$\int_{-\infty}^{\infty} H_{T(f_y)}^2 df_y = \frac{1}{L}, \text{ and} \quad (\text{II.11.a})$$

$$\int_0^{\infty} H_{w(f_x)}^2 df_x = \frac{1}{2W}. \quad (\text{II.11.b})$$

In addition, there is an assumption of white noise at the input of the detector preamplifier,

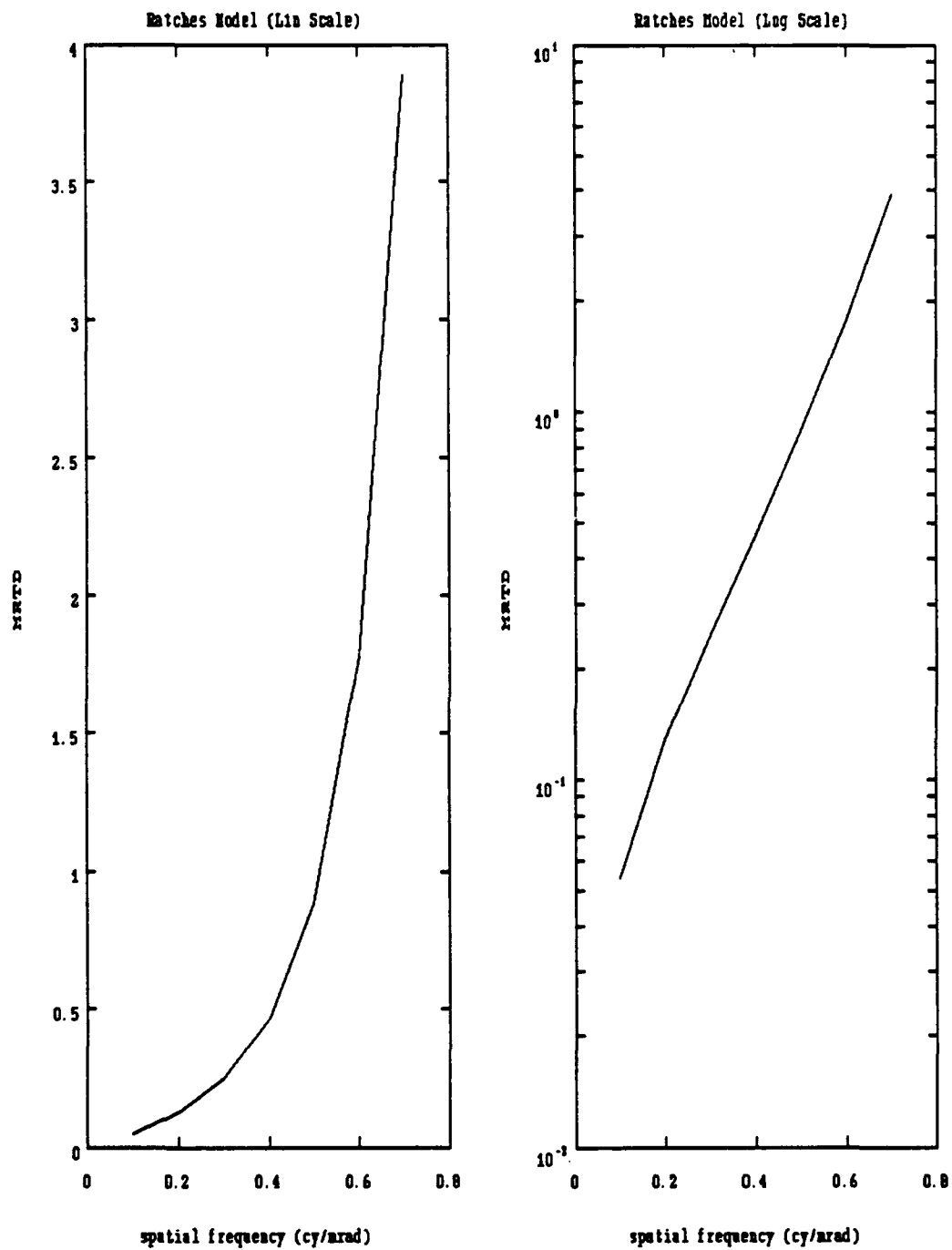


Figure II.3. Predicted MRTD using Ratches Model

$$\frac{S'_{i(f_x)}}{S'_{i(f_{rx})}} = 1 . \quad (\text{II.12})$$

Finally the response of the system in the low frequencies satisfies:

$$H_D = H_d = H_{ELECT} = 1 . \quad (\text{II.13})$$

By using these approximations, (II.8) reduces to:

$$\text{MRTD} = \frac{\pi^2 \Psi_{\text{NETD}}}{8 H_{D(f_{ox})}} \left[ \frac{\Delta y_i v_x}{F_r t_e \Delta f_n} \frac{2 f_{ox}^2}{7} \right]^{\frac{1}{2}} \quad (\text{II.14})$$

which leads, for the sample system, to a simple approximate MRTD expression:

$$\text{MRTD} = 0.49 \frac{f_{ox}}{H_{D(f_{ox})}} . \quad (\text{II.15})$$

Lloyd [Ref. 10, p. 190] obtains this simplified form by working strictly in the temporal frequency domain. This result, (II.15), convenient for some applications, is less reliable for the recognition and identification task at higher spatial frequencies than the more general form (II.8). The computer simulation of (II.15) is presented in Figure II.4 and compared with Ratches' predictions (II.8). A good agreement is observed in the low spatial frequencies while the effects of the approximations become noticeable in the high spatial frequencies.

Note that according to (II.15), the Ratches model [Ref. 5] predicts that the MRTD would go to zero as  $f_{ox} \rightarrow 0$ . Comparison

with actual measured MRTD data, e.g., as shown in Figure I.9 and Figure I.10, indicates that the low target frequency limit in the analytic expression (II.15) is not representative of actual TIS behavior. This is one of the motivating factors for the development of the visibility model proposed in the next chapter.

#### D. THE VORTMAN AND BAR-LEV MODEL FOR THE SAMPLE SYSTEM

Vortman and Bar-Lev [Ref. 8], introduced another approach for the MRTD model based on Ratches. The main difference with respect to the original model is the inclusion of an **adaptive** matched filter to represent the eye-brain system. This filter is matched to the fully degraded target signal rather than the traditional predetermined matched filter presented by Ratches. Also, in the Vortman and Bar-Lev model, the target is considered in its actual spatial description instead of assuming horizontal periodicity.

In general, any model based upon Ratches that uses the actual full target spectrum rather than its horizontally periodic approximation (A. 41) has an MRTD expression where:

$$\frac{\pi^2}{8 H_D(f_{ox})} \rightarrow \frac{1}{4 W \int_{-\infty}^{\infty} H_T(f_x) H_{mf}(f_x) [e^{(j2\pi f_x W)} - 1] df_x} \quad (\text{II.16.a})$$

and, therefore:

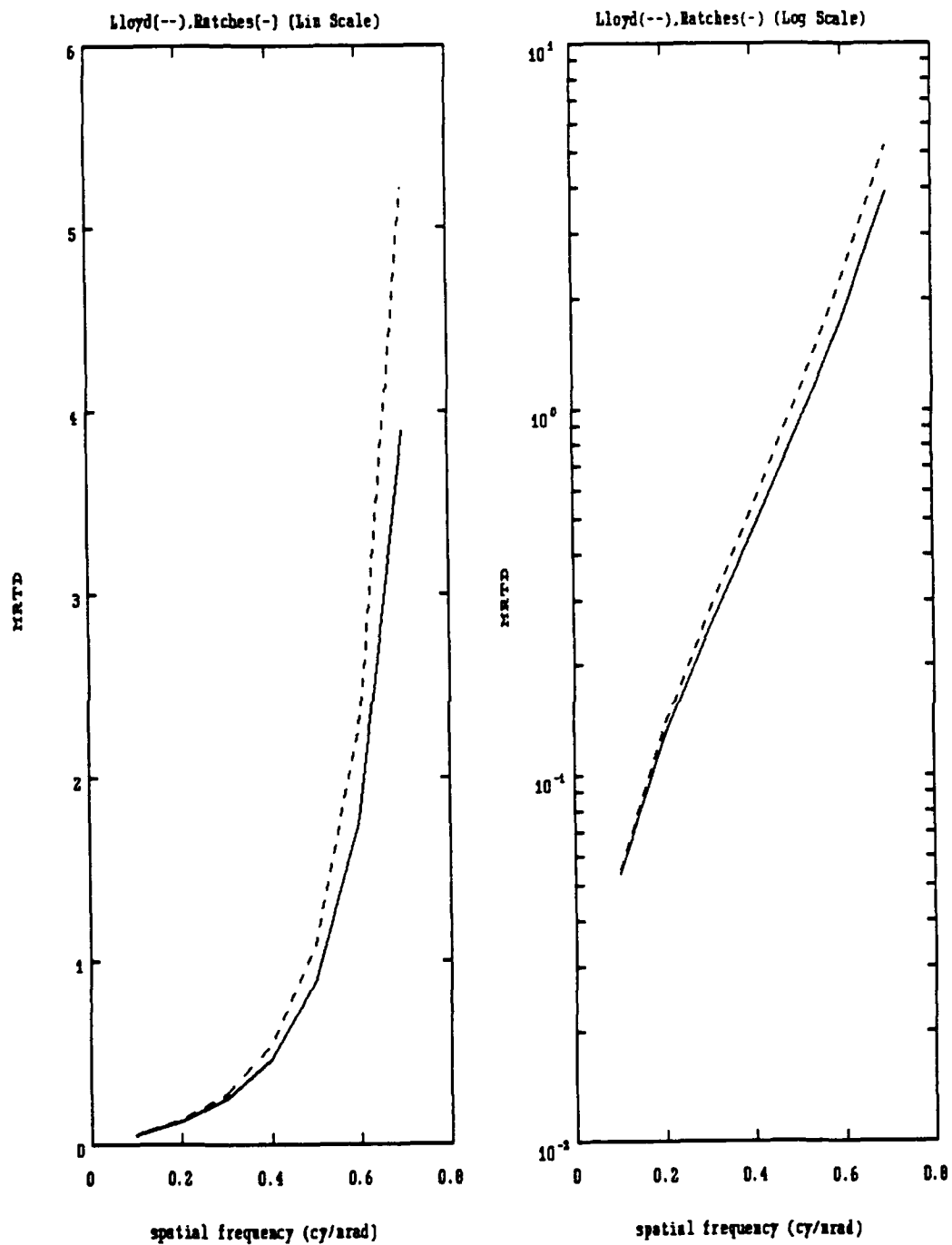


Figure II.4. Predicted MRTD. Lloyd's approximation vs. Ratches

$$\text{MRTD} = \frac{\Psi \text{NETD}}{A_T}$$

$$\frac{\left[ \frac{v_x \Delta y_i}{2 \Delta f_n F_r t_e} \int_{-\infty}^{\infty} \int_{-\infty}^{\infty} H_{\text{ELECT}}^2(f_x) H_d^2(f_x, f_y) H_{\text{mf}}^2(f_x, f_y) df_x df_y \right]^{\frac{1}{2}}}{\int_{-\infty}^{\infty} \int_{-\infty}^{\infty} H_T(f_x, f_y) H_d(f_x, f_y) H_{\text{mf}}(f_x, f_y) [e^{(j2\pi f_x u)} - 1] df_x df_y}$$

(II.16.b)

Equation (II.16.b) is a generic expression for the MRTD compatible with the Ratches [Ref. 5], Lloyd [Ref. 10], and Vortman and Bar-Lev [Ref. 4] models. What distinguishes these models, within the context of (II.16.b), are the matched filter ( $H_{\text{mf}}$ ) and the target spectrum ( $H_T$ ).

The adaptive matched filter employed in this model is a single bar of the target as in the Ratches model. However, it is different from the original, only degraded in the vertical direction (A.60), since both horizontal and vertical degradations are now included. Therefore, in the spatial frequency domain:

$$H_{\text{mf}}(f_x, f_y) = H_u(f_x) H_T(f_y) H_{\text{opt}}(f_x, f_y) H_{\text{det}}(f_x, f_y) H_{\text{ELECT}}(f_x) H_d(f_x, f_y) \quad (\text{II.17.a})$$

Although Vortman and Bar-Lev include a transfer function for the eye for (II.16), this is not considered here in order to maintain consistency with the other models analyzed.

These authors also discuss the consequences of employing white noise assumptions in the model. This implies working with a matched filter for white noise, instead of a theoretically more realistic matched filter for colored noise. The

Vortman and Bar-Lev analysis for the colored noise MRTD led to physically untenable conclusions, so the model was discarded.

Finally, after using the complete spectral description of the target and the adaptive matched filter, (II.8) is transformed into Vortman and Bar-Lev model for white noise:

$$\text{MRTD} = \frac{\Psi \text{NETD}}{A_T}$$

$$= \frac{\left[ \frac{v_x \Delta y_i}{2 \Delta f_n F_r t_e} \int_{-\infty}^{\infty} \int_{-\infty}^{\infty} H_{\text{ELECT}}^4(f_x) H_d^4(f_x, f_y) H_w^2(f_x) H_T^2(f_y) H_{\text{opt}}^2(f_x, f_y) H_{\text{det}}^2(f_x, f_y) df_x df_y \right]^{\frac{1}{2}}}{\int_{-\infty}^{\infty} \int_{-\infty}^{\infty} H_T(f_x, f_y) H_w(f_x) H_T(f_y) H_D^2(f_x, f_y) [e^{(j2\pi f_x u)} - 1] df_x df_y}$$

(II.17.b)

which is plotted in Figure II.5 versus the Ratches model (II.8). It can be observed that here is a substantial disagreement between both models, specially as spatial frequency increases.

The reader can confirm that (II.17.b) is in agreement with equation 16 from [Ref. 8] after noting that  $t_d = \Delta x / v_x$ .

The three models considered in this chapter represent different concepts of visual perception. In all three cases, discrepancies between predicted and measured data persist. The need for improved modeling is the motivation for the proposed models introduced in the next chapter.

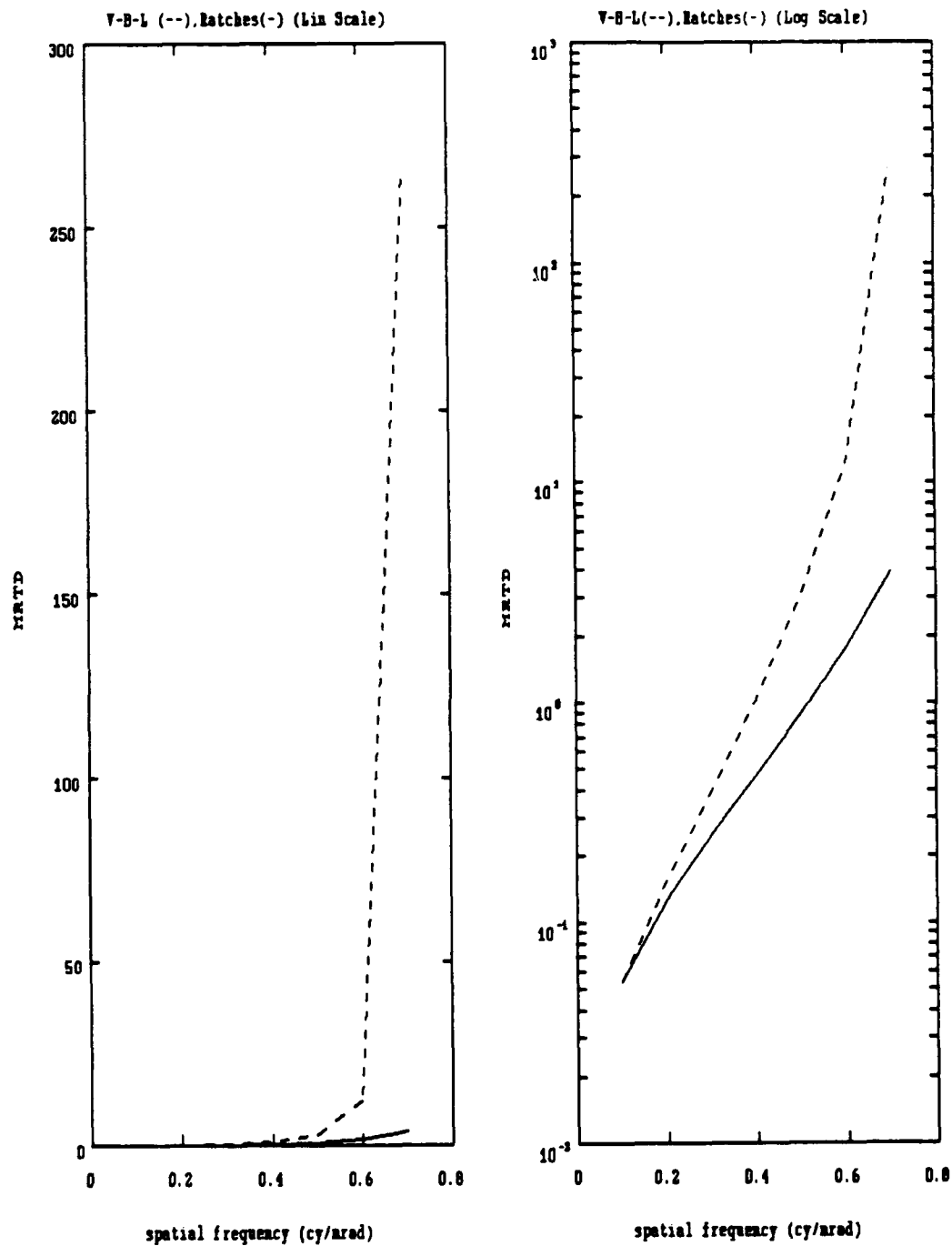


Figure II.5. Predicted MRTD. Vortman and Bar-Lev vs. Ratches



### III. PROPOSED MRTD MODELS

#### A. MODIFIED VORTMAN AND BAR-LEV MODEL FOR THE SAMPLE SYSTEM

As presented in Appendix A, the Ratches model is based on the assumption of white noise at the input of the TIS. The transfer function of the system obviously colors the displayed noise as stated by Vortman and Bar-Lev, and therefore the use of a matched filter for white noise (impulse response equal to the spatially reversed displayed signal) should not be considered. However, practical reasons require the assumption of a matched filter for the white noise case.[Ref. 8]

If the input noise is assumed to be white as well as the displayed noise, this implies the system's MTF does not affect the noise spectral distribution. It follows that the same criterion must be employed in the definition of the matched filter, and no degradation should be considered for the original bar in the direction where the noise is assumed to occur (horizontal). Therefore, presenting a horizontally degraded adaptive matched filter under white noise assumptions is a contradiction that leads to inaccurate modeling. This was evident in the computer simulations shown in Figure I.7 and Figure I.8.

Two different modifications can be attempted on the Vortman and Bar-Lev model:

1. Matched Filter undegraded only in the horizontal direction (where the considered noise occurs):

$$H_{mf}(f_x, f_y) = H_w(f_x) H_T(f_y) H_D(f_y) \quad (\text{Ratches}) \quad (\text{III.1.a})$$

which leads to a modified Vortman and Bar-Lev MRTD (Mod. No.1) after substitution into (II.16.b):

$$\text{MRTD} = \frac{\Psi \text{NETD}}{A_T}$$

$$\cdot \frac{\left[ \frac{v_x \Delta y_i}{2 \Delta f_n F_r t_e} \int_{-\infty}^{\infty} \int_{-\infty}^{\infty} H_{\text{ELECT}}^2(f_x) H_d^2(f_x, f_y) H_w^2(f_x) H_T^2(f_y) H_D^2(f_y) df_x df_y \right]^{\frac{1}{2}}}{\int_{-\infty}^{\infty} \int_{-\infty}^{\infty} H_T(f_x, f_y) H_w(f_x) H_T(f_y) H_D(f_x, f_y) H_D(f_y) [e^{(j2\pi f_x W)} - 1] df_x df_y}$$

(III.1.b)

where, as explained in the early part of Appendix A, the single-bar normalized spectrum  $H_w(f_x)$  can supplant the four-bar normalized spectrum  $H_T(f_x)$  without loss in generality.

2. Matched Filter undegraded in both horizontal and vertical directions:

$$H_{mf}(f_x, f_y) = H_w(f_x) H_T(f_y) \quad (\text{III.2.a})$$

which leads to a second modified Vortman and Bar-Lev MRTD (Mod. No. 2):

$$\text{MRTD} = \frac{\Psi \text{NETD}}{A_T}$$

$$\cdot \frac{\left[ \frac{v_x \Delta y_i}{2 \Delta f_n F_r t_e} \int_{-\infty}^{\infty} \int_{-\infty}^{\infty} H_{\text{ELECT}}^2(f_x) H_d^2(f_x, f_y) H_w^2(f_x) H_T^2(f_y) df_x df_y \right]^{\frac{1}{2}}}{\int_{-\infty}^{\infty} \int_{-\infty}^{\infty} H_T(f_x, f_y) H_w(f_x) H_T(f_y) H_D(f_x, f_y) [e^{(j2\pi f_x W)} - 1] df_x df_y}$$

(III.2.b)

Figure III.1 shows the simulation of the first modified model. The predicted MRTD is coincident with the one obtained by Ratches.

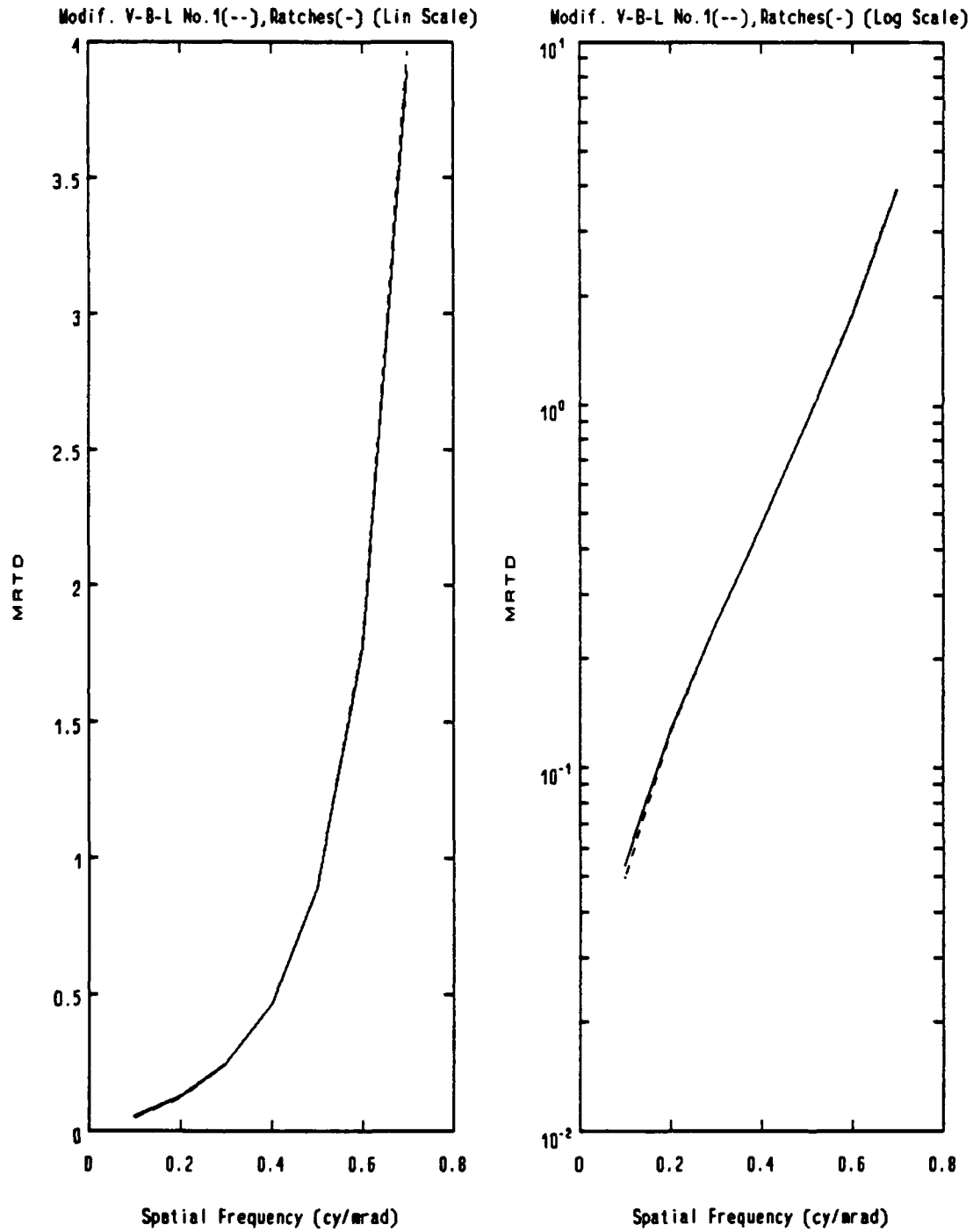


Figure III.1. Predicted MRTD using modification No. 1 on V-B-L

Figure III.2 shows the second modification, where the results observed are essentially the same as for the first. This demonstrates that the issue of degradation along the vertical direction is irrelevant for a typical TIS like the one employed in this work and that the Ratches simplifications are correct in that sense.

#### B. A VISIBILITY MODEL FOR MRTD MEASUREMENTS

Today fairly successful MRTD predictors appearing in the literature [Ref. 5], [Ref. 8], [Ref. 9], [Ref. 10, p. 190] are all based on a signal-to-noise (S/N) analysis. The predicted MRTD is subsequently determined by a threshold condition on the S/N. In most cases these models generate an MRTD which is directly proportional to the NETD. This parameter is defined as the temperature difference between a large target and background which leads to a  $S/N=1$  under conditions that a special reference filter is employed. The reference filter has the effect of desensitizing the NETD to spatial frequency effects inherent to the system. Excluding the NETD, the rest of the MRTD will depend on inherent spatial frequency effects. This motivates a proposed generic form for the MRTD:

$$MRTD_{(f_{ox})} = MRTD_{(f_{ox}=0)} \text{ function}_{(system\ MTFs)}$$

which does not appear to be 100% consistent (see II.15) with previous MRTD predictors discussed in the literature. Nonetheless this form has significant physical appeal.

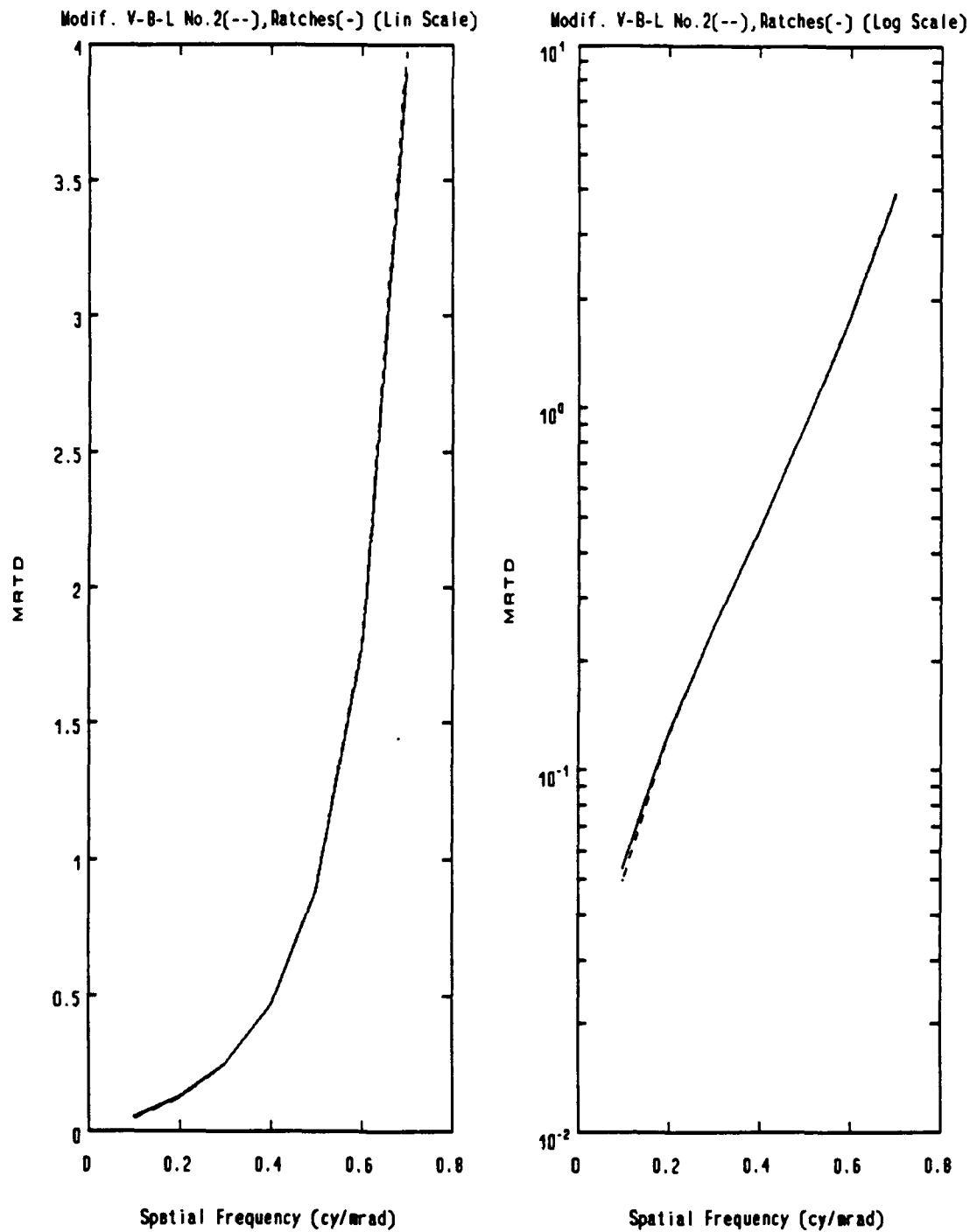


Figure III.2. Predicted MRTD using modification No. 2 on V-B-L

In the low frequency limit the MRTD tends to be more optimistic than the NETD due to eye-brain matched filtering [Ref. 5], [Ref. 8]. In these established models the complex [Ref. 14] and controversial [Ref. 25] task of treating eye-brain filtering has to be addressed.

In the visibility model to be discussed, the complexity of eye-brain modeling is sidestepped by not dealing with the NETD directly. The low-frequency MRTD, which serves partially as an NETD substitute, also incorporates effects of the MRTD decision process. For the standard subjective MRTD this involves eye-brain filtering. The analysis for the visibility model concentrates on contrast reduction due to spatial frequency limiting factors. Direct consideration of noise is obviated.

This proposed model leads to a simpler development for an MRTD predictor and appears to provide a more reliable tool for forecasting the performance of a TIS.

As pointed out by Lloyd [Ref. 10, p. 210], the modulation transfer function "correlates with recognition and identification performance in noise-free imagery". The degradation produced by the system to a rectangular wave in the horizontal direction is considered and the amplitude of the resulting wave is compared to a critical value to determine the recognition of the target. Hypothetically, this threshold for recognition could eventually be expressed as a function of the NETD and other system parameters.

Figure III.3 summarizes the salient features of the model. The overall MTF is obtained from subsystem effects. The thermal rectangular wave source is characterized by a period  $1/f_{ox}$  and temperature difference  $\Delta T$ . The response's amplitude  $\Delta T_s$  is guaranteed to be less than  $\Delta T$ . The numerical curves discussed in the next paragraph were obtained by applying the computation algorithm shown in Appendix B on the sample system described in Appendix D.

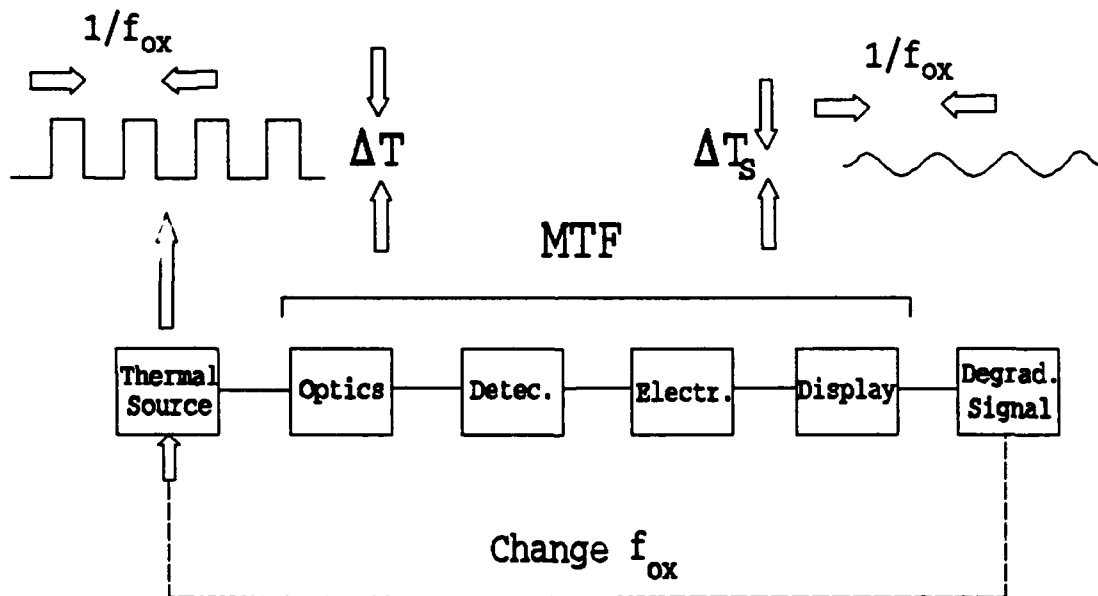


Figure III.3. Modified Visibility Model Concept

The upper half of Figure III.4 shows the approximation to a rectangular wave of spatial frequency equal to, e.g., 0.7 [cy/mrad] employing the first five harmonics of its Fourier series expansion (undegraded target). The lower half of III.4

shows the degraded version of that signal after passing through the TIS (degraded target). Besides a loss of the original shape, its amplitude has decreased.

Upper and lower portions of Figure III.5 show the individual 5 harmonics in the undegraded and degraded targets respectively (the latter shows the four highest harmonics essentially canceled).

Since the degraded target is the available signal for the observer, it provides distorted information on what is the actual difference in temperature in the target. If this measured temperature difference is called  $\Delta T_s$ , then a parameter  $\alpha$  that relates the measured temperature difference to the actual one ( $\Delta T$ ) can be defined:

$$\alpha = \frac{\Delta T_s}{\Delta T} . \quad (\text{III.3})$$

For the sample system, this parameter  $\alpha$  is plotted versus spatial frequencies in Figure III.6.

It is reasonable to assume that there is a minimum or critical measured apparent temperature difference ( $\Delta T_{sc}$ ) that an observer can resolve. By definition  $\Delta T_{sc}$  corresponds to the condition  $\Delta T = \text{MRTD}$ . Thus:

$$\text{MRTD} = \frac{\Delta T_{sc}}{\alpha} . \quad (\text{III.4})$$

Figure III.7 shows the resulting predictions compared with the Ratches model for the sample system, with  $\Delta T_{sc} = 0.23^\circ\text{C}$ . This critical temperature difference produced fairly close



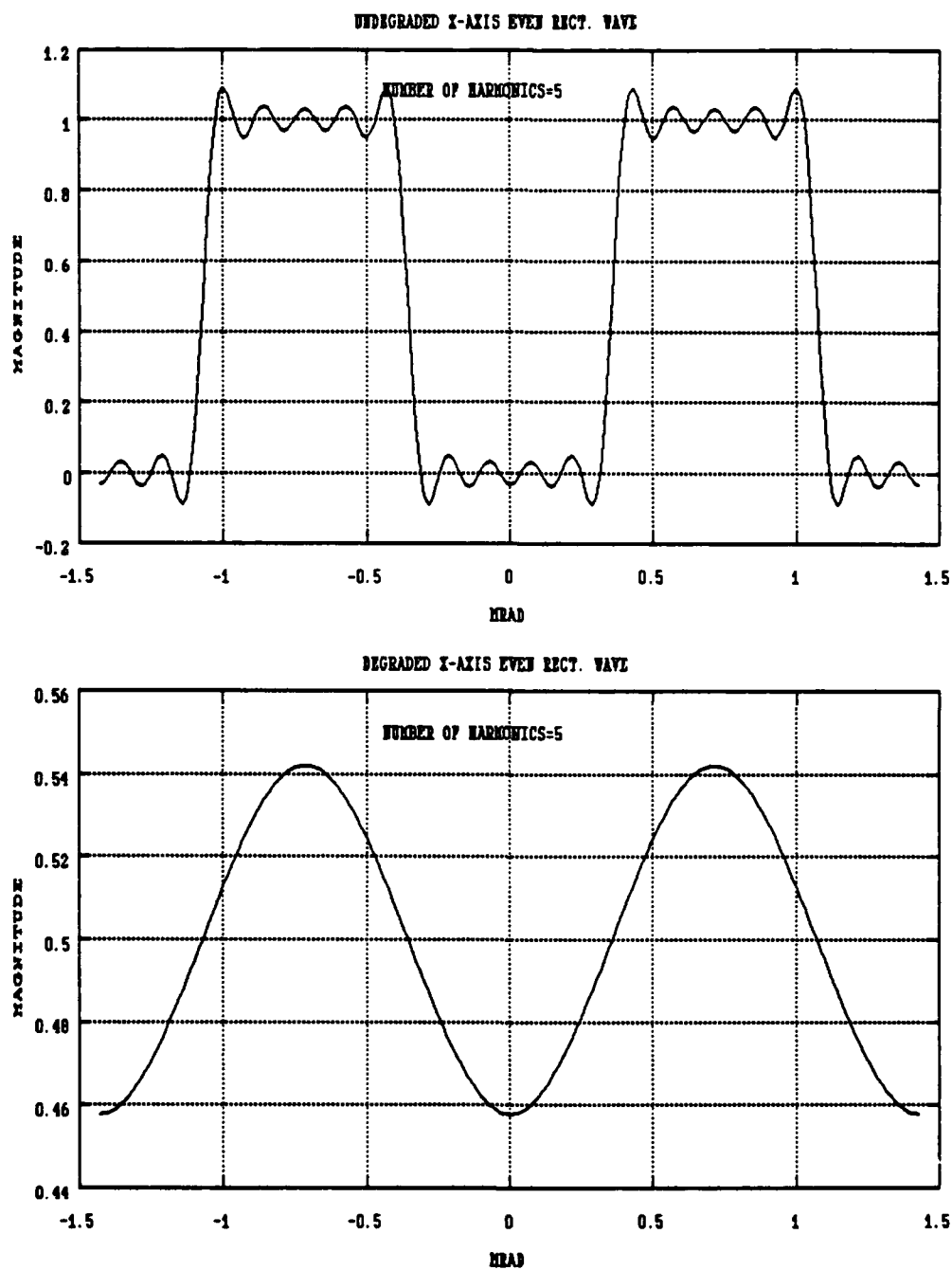


Figure III.4. MTF degradation of a rectangular wave

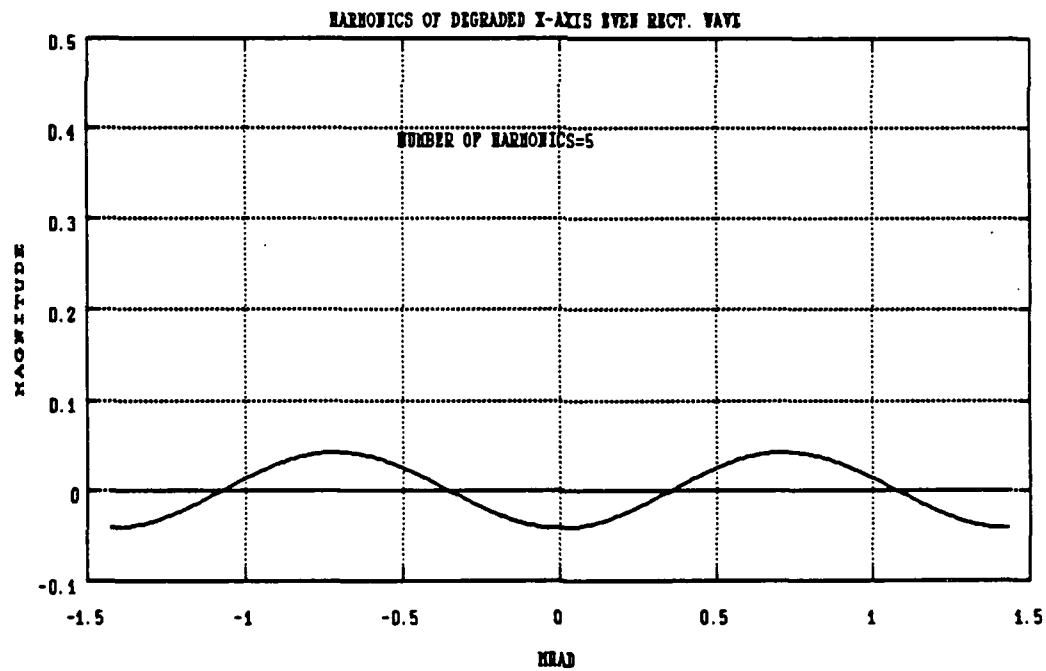
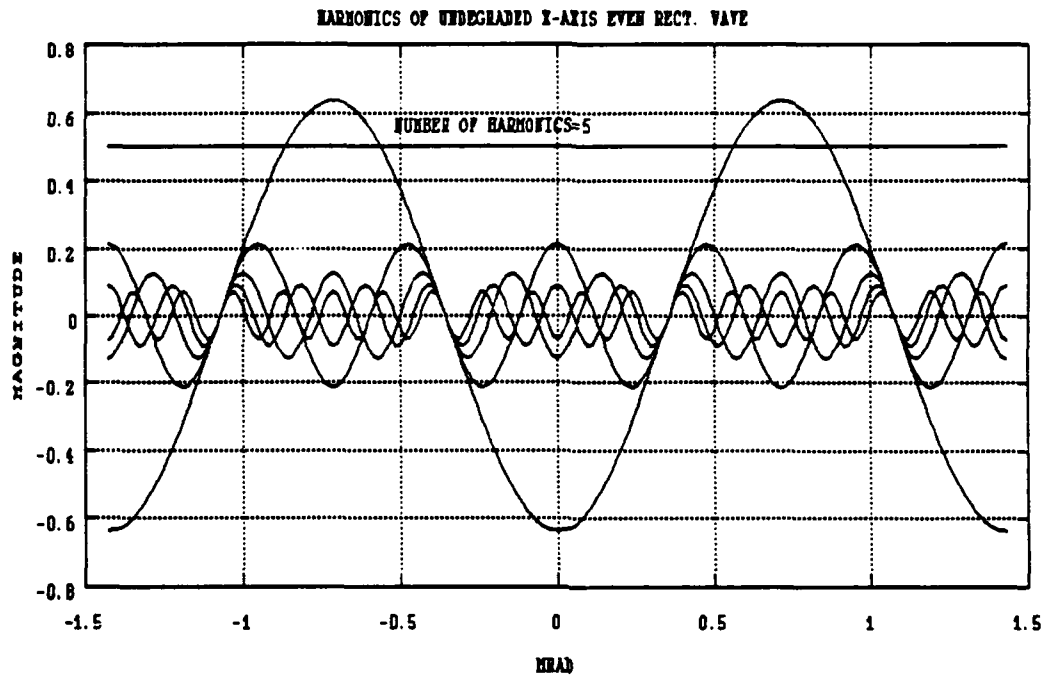


Figure III.5. Undegraded and degraded target harmonics

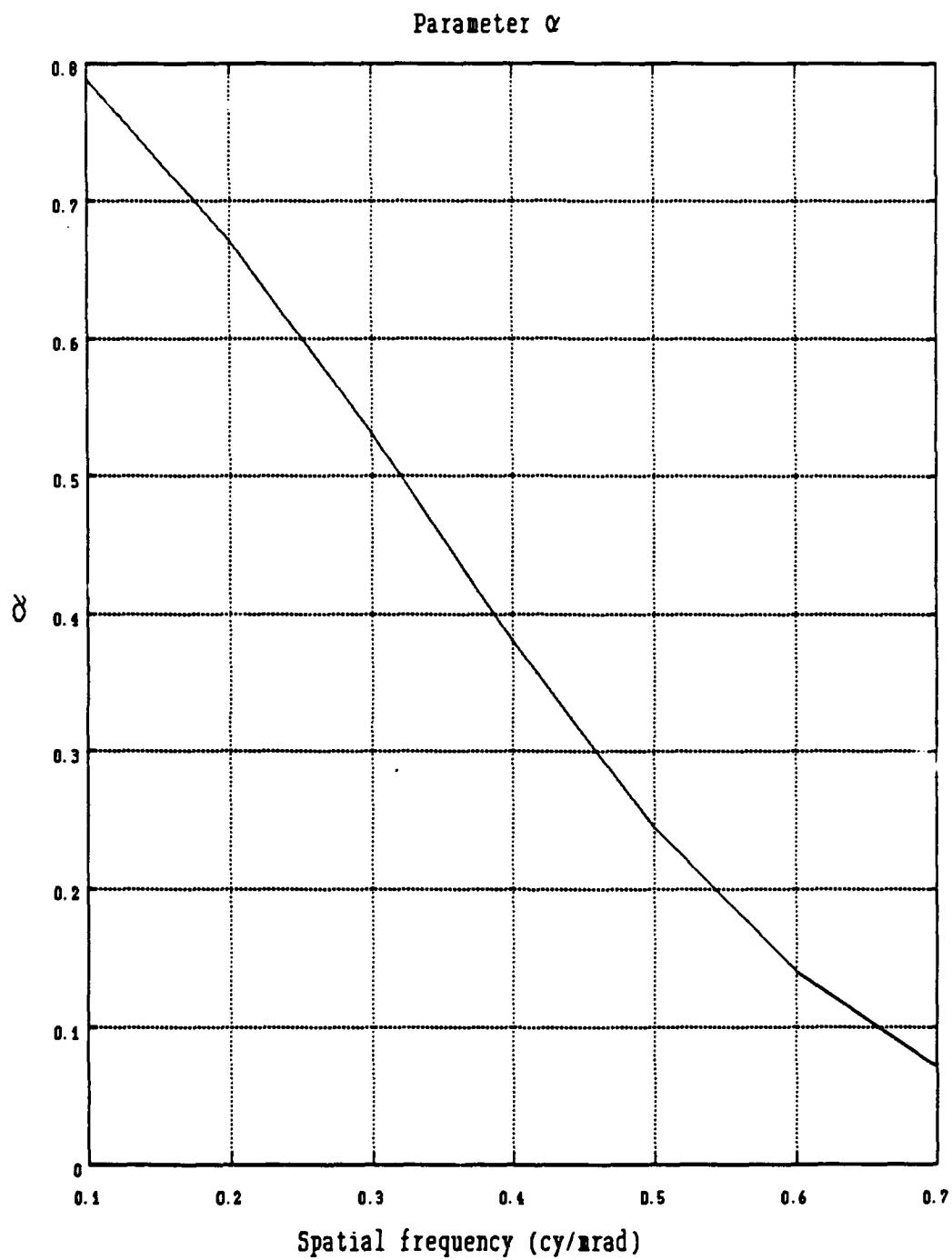


Figure III.6. Parameter  $\alpha$

agreement with the Ratches model. In order to relate the visibility model to previous descriptions,  $\Delta T_{sc}$  can be expressed as:

$$\Delta T_{sc} = \frac{NETD}{\beta} \quad (III.5)$$

where  $\beta$  should be an empirical factor dependent on the measurement process for recognition. Then,  $\Delta T_{sc}$  clearly becomes a new NETD-like parameter where the signal-to-noise ratio improvement performed by the eye-brain system and the display effects are included. For the simulation of this model on the sample system, the  $\beta$  calculated from the NETD (see end of Chapter II, Section A) was  $\beta=1.58$ .

The curves shown in Figure III.7 demonstrate several noteworthy trends. At low frequencies the visibility model is not as optimistic as the Ratches model. At higher frequencies this relation is reversed and the visibility model tends to be more optimistic than the Ratches model. Figure I.9 and Figure I.10 show that measured data behaves similarly when compared with the Ratches model. Therefore the visibility model has excellent potential for serving as a more reliable performance forecaster than the Ratches model.

#### C. INCLUSION OF SAMPLING ARTIFACTS. EFFECTS ON THE RATCHES MODEL

For systems considered here, as represented in Figure A.1, the main sampling effect takes place along the vertical

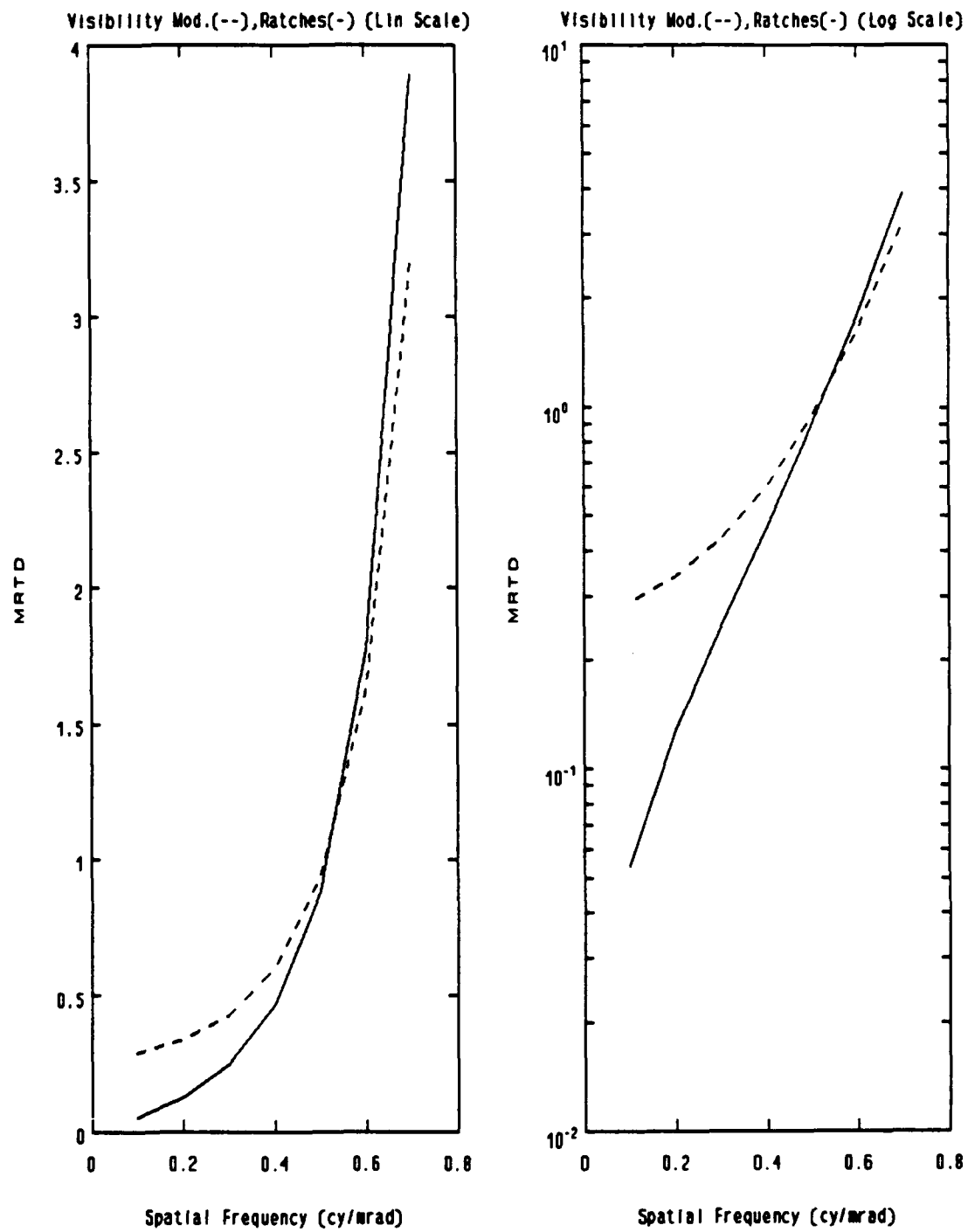


Figure III.7. Visibility MRTD model

direction. This is due to the horizontal scanning being performed on lines separated by an angular distance  $\Delta y_i$  mrad. This consequently leads to a periodicity of the spectrum of the observed target in the vertical direction. The target spectrum repeats itself every  $1/\Delta y_i$  [cy/mrad]. In Appendix C, the full 2D spectrum of the four bars is derived. It is noted that, consistent with specifications in Appendix D for the sample system, the center-to-center spacing of the detectors is taken to be equal to the vertical detector width. In a well-designed system, the main energy carried by the aliases created by sampling should lay in the region beyond the cutoff frequency of the overall MTF. In order to evaluate the importance of this unwanted effect, a periodic spectrum is considered here for MRTD modelling. Figure III.8 shows the periodic (dashed) and aperiodic (solid) vertical spectrum of a standard target of 0.7 [cy/mrad] for the sample system (Appendix D). Figure III.9 shows how the system's MTF minimizes this effect.

As an example, Figure III.10 shows the plot of the MRTD according to Ratches, using a the new sampled  $H_{T(f_y)}$ . In this case, as expected, there is no essential difference with respect to the original model. This shows that the sample system is correctly designed since the modulation transfer function is such that the periodic spectra are essentially filtered out and, therefore, sampling effects can be neglected.

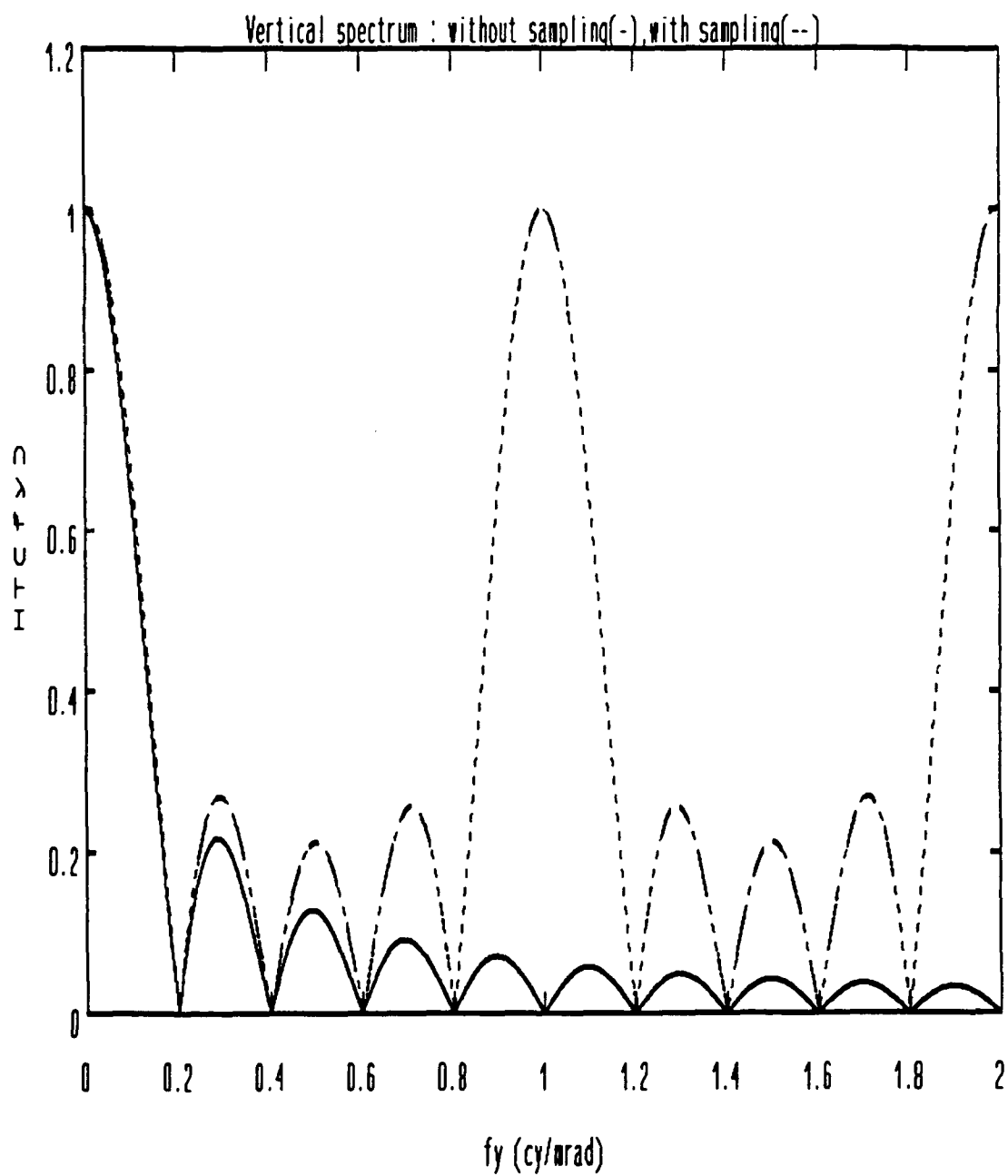


Figure III.8. Effects of sampling on vertical spectrum

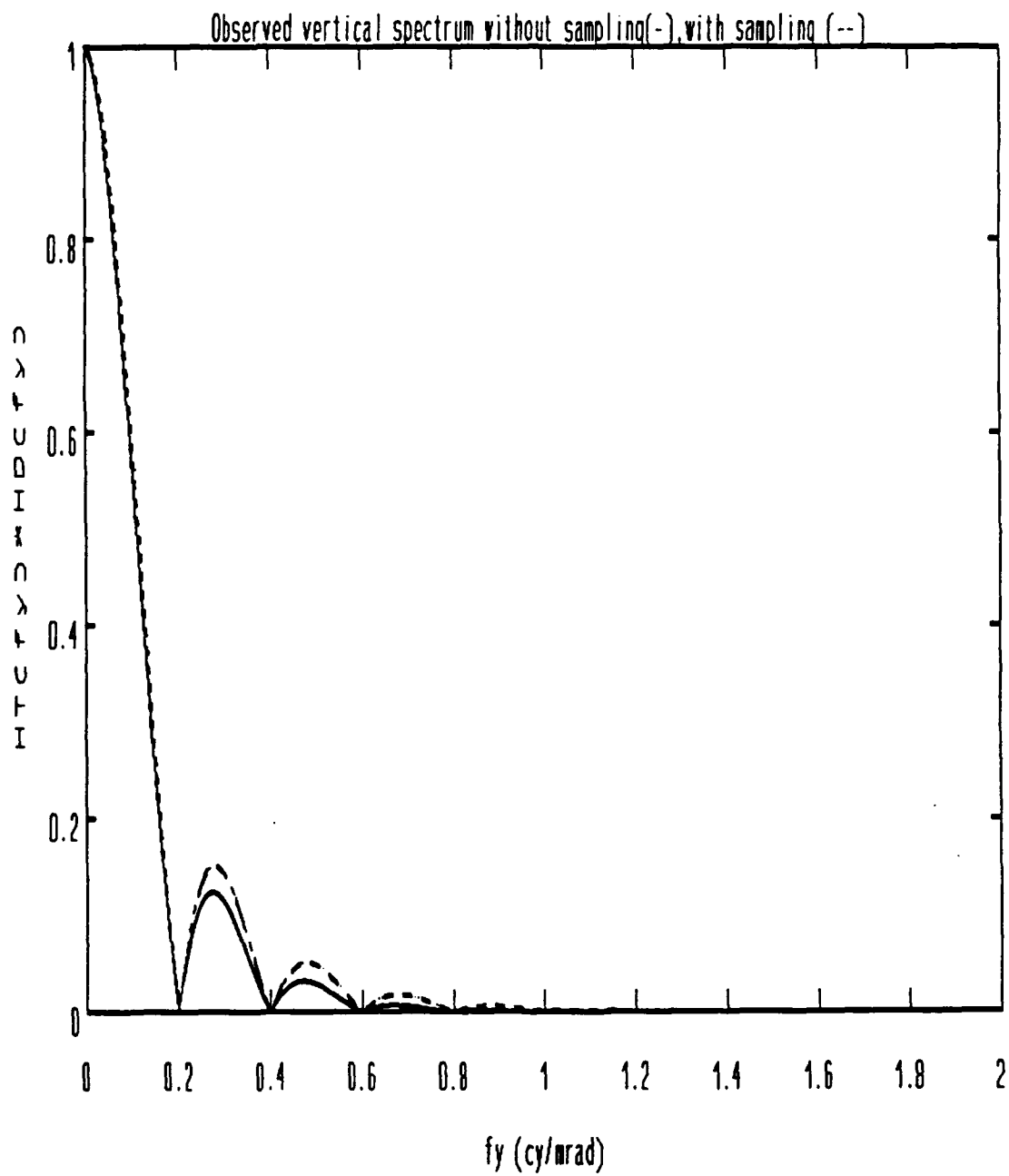


Figure III.9. MTF effects on vertical spectrum



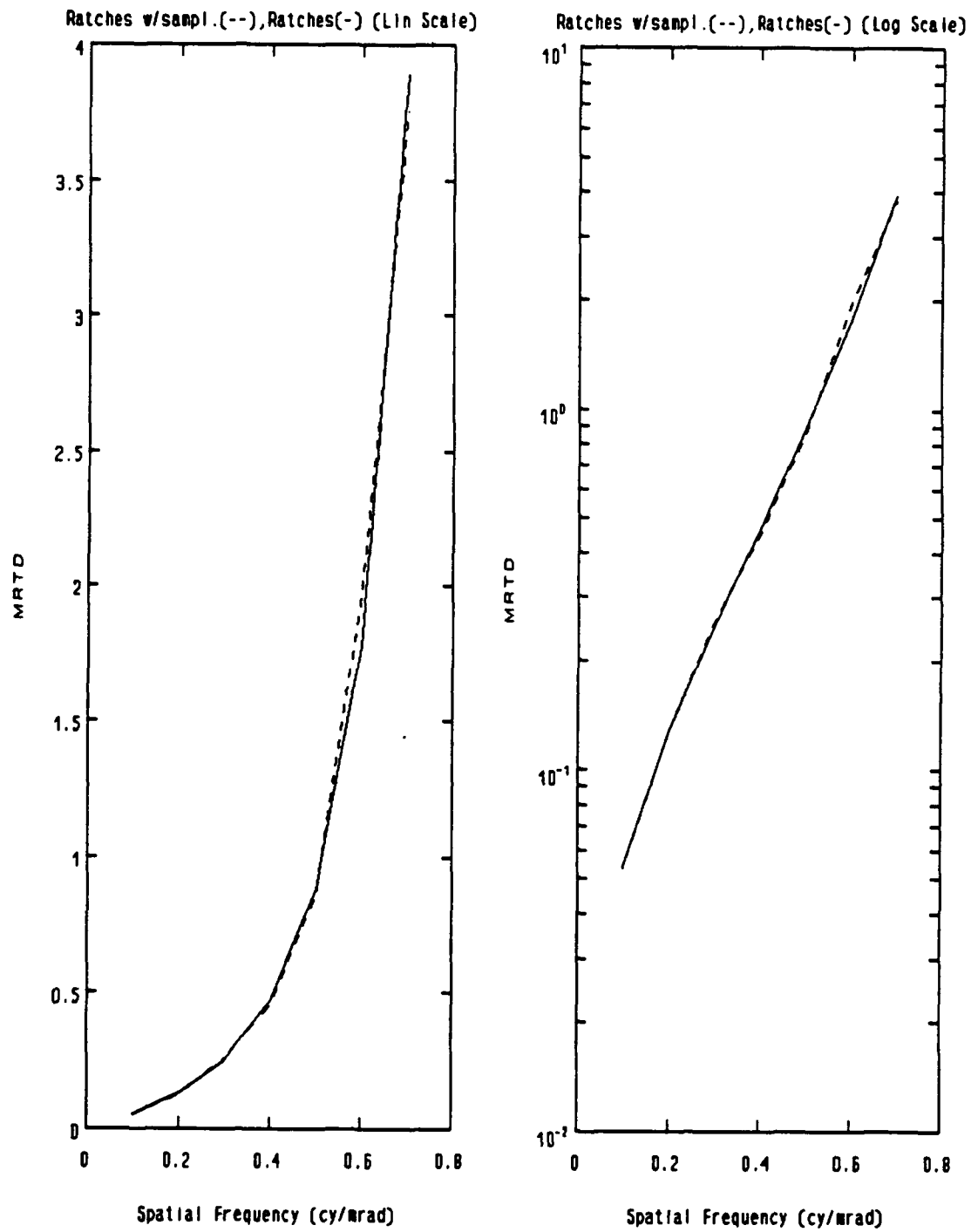


Figure III.10. Sampling artifacts on Ratches' MRTD prediction

#### IV. COMPARATIVE ANALYSIS AND CONCLUSIONS

Some of the conclusions presented here are based on computer simulations performed on the sample system specified in Appendix D.

As expected, the Lloyd model demonstrates the best agreement with the Ratches model at low spatial target frequencies. However, as observed, there is a physical inconsistency with the Ratches model at low frequencies. This led to the generally recognized conclusion that a model that provides a higher estimation for the MRTD at low frequencies is needed.

The Adaptive Matched Filter (AMF) model by Vortman and Bar-Lev employs a mathematically more technical application of the matched filter treatment for the eye-brain than does the Ratches model. Comparison between simulations and actual measured data suggest that Vortman and Bar-Lev treatment produces an unwanted and magnified disagreement between model and reality in the high frequencies without obtaining any improvement in the lower ones. The conclusion from this comparison is that the eye-brain is better modeled as a matched filter for the undegraded target signal, as originally proposed 30 years ago by Ratches.

It was found in Chapter II and Chapter III, by comparison of computer simulations for the sample system, that use of the

exact four-bar target spectrum is not really necessary. Not only can the spectrum be reasonably approximated by an infinite square wave but Ratches' use of only the first harmonic turns out to be quite good. This was demonstrated in Chapter III, Section A, by redefining Vortman and Bar-Lev matched filter (both modifications No. 1 and No. 2). The results from the new models essentially coincide with the Ratches model. This proves that the periodic assumption for the target and the use of the first harmonic proposed by Ratches (A.41) is a correct engineering approach. The results obtained from modification No. 2 to Vortman and Bar-Lev confirm the general irrelevancy of including degradation effects along the vertical axis within the matched filter as in the Ratches model.

The proposed Modified Visibility model brings up a very simplistic concept of the perception process. Although the feasibility of a universally valid parameter  $\beta$  requires additional research, the results seem to be in better agreement with physical measurement than the Ratches model. Since this has been only tested on the sample system, further experimental simulations on different systems must be pursued. It should be noted that this model does not suffer from the unphysical condition that the low frequency limit for the MRTD equals zero. It was demonstrated in Chapter III, Section C that the Ratches model exhibits this defect. The possibility that this problem is endemic to all models based on a S/N

calculation needs to be studied. Furthermore the general development of the visibility model makes no assumptions on the nature of the decision process. For this reason the modified visibility model has significant unexplored potential as a mathematical framework for objective MRTD modeling.

Finally, it was demonstrated in Chapter III, Section C that the inclusion of sampling artifacts, tested on the sample system, hardly affected the MRTD calculation. In order to evaluate the impact sampling effects will have on the MRTD calculation for an arbitrary system, the approach presented in Chapter III, Section C should be applied.

For readers interested in a more detailed description of the computer simulation algorithm a flowchart is provided in Appendix B.

## **APPENDIX A - INTERPRETATION OF THE RATCHES MODEL**

The inclusion of this appendix serves two important functions. First, it provides the necessary background to make this thesis fairly self-contained. Second, the evolution of concepts surveyed here includes additional physical interpretations not provided in the original manuscript [Ref. 5]. From a pedagogical point of view these additional enhancements are essential to the fundamental understanding of the original work.

The model presented by the NIGHT VISION LABORATORY in 1975 [Ref. 5], better known as the Ratches model, predicts system Noise Equivalent Temperature Difference (NETD), Modulation Transfer Function (MTF), Minimum Detectable Temperature Difference (MDTD), and Minimum Resolvable Temperature Difference (MRTD) for any scanning thermal imaging system. An important characteristic of this model is the fact that it represents the image processing that takes place in the eye-brain system by a matched filter [Ref. 5], [Ref. 8]. Although this assumption may not exactly correspond to what really occurs in the complex process of visual recognition, [Ref.12], [Ref. 13], [Ref. 14], [Ref.15], it has shown a remarkable success and has been widely accepted by the infrared community. The present appendix follows the steps presented by Ratches and Lawson in the report "The Fundamentals of Thermal

Imaging Systems" produced by the NAVAL RESEARCH LABORATORY in 1979 [Ref. 30].

#### A. PRELIMINARIES

From linear systems theory, it is known that the output signal from a system is equal to the input signal convolved with the impulse response of the system, i.e.,

$$i_{o(t)} = i_{i(t)} \star h_{(t)} = \int_{-\infty}^{\infty} i_{(\tau)} h_{(t-\tau)} d\tau. \quad (A.1)$$

where the subscript i stands for input and the subscript o for output.

In the frequency domain, the Convolution Theorem can be applied to (A.1) to obtain the expression:

$$I_{o(f)} = I_{i(f)} H_{(f)}, \quad (A.2)$$

where  $I_{o(f)}$  is the Fourier transform of  $i_{o(t)}$  and  $H_{(f)}$  is the transfer function of the linear system.

If cascaded systems are considered, the Fourier transform of the output signal is:

$$I_{o(f)} = I_{i(f)} H_{1(f)} H_{2(f)} \dots \quad (A.3)$$

where  $H_{1(f)}$  and  $H_{2(f)}$  are the transfer Functions of the first and second systems respectively.

To characterize the effects of noise generated by a wide-sense stationary process such as that found in most thermal imaging systems, the autocorrelation function of the noise

needs to be employed. This operation, for finite power signals, is defined as:

$$R_f(\tau) = \lim_{T \rightarrow \infty} \int_{-\frac{T}{2}}^{\frac{T}{2}} f_{(t)}^* f_{(t+\tau)} dt \quad (\text{A.4.a})$$

which can be represented for the real noise signal  $n_{(t)}$

$$R_{(t)} = \langle n_{(t)} n_{(t+\tau)} \rangle . \quad (\text{A.4.b})$$

where brackets indicate average. A random process is said to be wide-sense stationary if the statistics corresponding to average and autocorrelation do not depend on the location of the time origin [Ref. 31]. Expressions (A.4) have already incorporated this assumption.

The power spectral density (PSD) of the noise can then be found by taking the Fourier transform on the autocorrelation function (Wiener-Khintchine Theorem [Ref. 31, p. 458]):

$$S_{(f)} = \mathcal{F} \{R_{(t)}\}. \quad (\text{A.5})$$

After passing through a linear system, the output PSD is [Ref. 32]:

$$S_{o(f)} = S_{i(f)} H_{(f)}^2. \quad (\text{A.6})$$

The time variance of a measured signal due to the noise generated by a random process of mean equal to zero is related to the noise spectral density as follows:

$$\sigma = \sqrt{\langle n_{(t)}^2 \rangle} \quad (\text{A.7.a})$$

or, in the frequency domain,

$$\sigma^2 = \int_{-\infty}^{\infty} S_{(f)} df. \quad (\text{A.7.b})$$

To avoid the use of negative frequencies, a one-sided noise PSD,  $S'_{(f)}$ , is defined such that:

$$\sigma^2 = \int_0^{\infty} S'_{(f)} df. \quad (\text{A.8})$$

A matched filter [Ref. 30] "is a filter whose response function is a delayed (shifted), time-reversed (spatially reversed) version of the signal". Thus, if the signal is defined as  $i_{(t)}$ , the impulse response of a matched filter results:

$$h_{m(t)} = K i_{(\tau - t)} \quad (\text{A.9})$$

where  $K$  is a constant. For convenience this arbitrary constant will be taken to have the ideal value 1 and units of  $(\text{time})^{-1}$ . This kind of filter maximizes the signal-to-noise ratio at time  $t=\tau$ , considering, a) the signal output is the peak of the autocorrelation of the input signal and b) the input noise that assumed to be additive and white. This assumption is approximately true for thermal, shot, generation-recombination and radiation (or photon flux) types of noise [Ref. 33].



Any  $1/f$  noise component in the low frequencies and the high-frequency roll-off are ignored in the model. Assuming  $\tau=0$ , the transfer function of such a matched filter is:

$$H_{m(f)} = K I_{(f)}^* \quad (\text{A.10})$$

The final MRTD expression depends only on the magnitude of the matched filter. Since linear transform theory predicts that the magnitude of a transfer function does not depend on a shift in the corresponding impulse response, the assumption is justified.

#### **B. DERIVATION OF THE NOISE EQUIVALENT TEMPERATURE DIFFERENCE (NETD)**

The definition of NETD employed in this model is [Ref. 30] "that input temperature difference for a 'large' target (a large target being one whose size is large relative to the system response function) which is required to generate a signal (voltage amplitude) just prior to the display (or after the detector preamplifier) which is just equal to the rms noise (voltage) at that point, assuming that the filtering action of the electronics prior to the measurement point corresponds to that of a 'standard' filter." In other words, the NETD is the temperature difference between a large uniform target (which implies low spatial frequency) and a uniform background that produces a signal-to-noise ratio equal to 1 at that point.

It can be assumed (Figure A.1) that each detector plus the associated preamplifier form a linear system with a impulse response function:

$$h_{\text{DET-ELECT}}(\lambda, t) = r_{(\lambda, t)} \star h_{\text{ELECT}}(t) \quad [\text{volts/watt}], \quad (\text{A.11})$$

where  $r_{(\lambda, t)}$  is the response of the detector [volts/watt] and  $h_{\text{ELECT}}(t)$  represents the response of the preamplifier and the associated circuitry. The signal incident onto the detector can be represented as a function of  $\lambda$  and  $t$ , in which the wavelength and time dependence are separable:

$$P_{(\lambda, t)} = \Delta\phi_{(\lambda)} i_{(t)} \quad [\text{watts}/\mu\text{m}] \quad (\text{A.12})$$

The quantity  $P_{(\lambda, t)}$  can be considered as the time-varying spectral radiant flux falling on a detector. The function  $\Delta\phi_{(\lambda)}$  is the wavelength dependent part [watts/ $\mu\text{m}$ ], and  $i_{(t)}$  a normalized (peak value equal to one) time function. The response at the detector is then obtained by extending the linear systems result (A.11) and integrating over wavelength. The output voltage  $v_{s(t)}$  from each detector-amplifier system is obtained as:

$$v_{s(t)} = \int_0^{\infty} \Delta\phi_{(\lambda)} i_{(t)} \star r_{(\lambda, t)} \star h_{\text{ELECT}}(t) d\lambda \quad [\text{volts}] \quad (\text{A.13})$$

which corresponds to a detector-amplifier system like the one presented in Figure A.1.

To simplify the expression, it can be assumed that the one-dimensional transform of  $r_{(\lambda, t)}$  is separable into a wavelength and a frequency dependent part  $R_{(\lambda)}$  and  $R_{(f)}$ , such that:

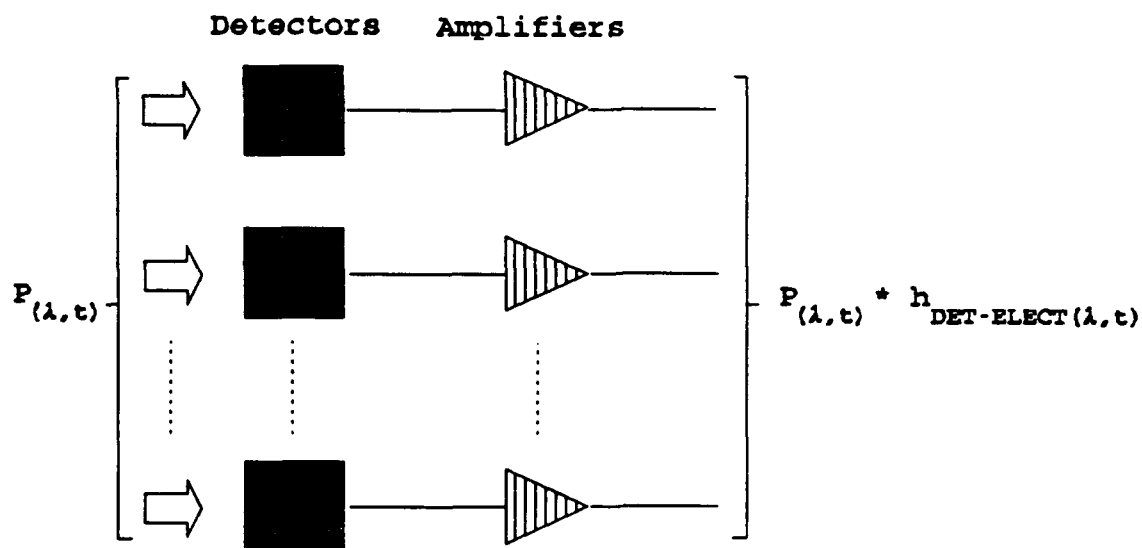


Figure A.1. Detector-Amplifier system

$$\mathcal{F}_t \{x_{(\lambda, t)}\} = R_{(\lambda, f_r)} \frac{R_{(\lambda, f)}}{R_{(\lambda, f_r)}}, \quad (\text{A.14.a})$$

where:

$$R_{(\lambda)} = R_{(\lambda, f_r)}, \quad (\text{A.14.b})$$

and

$$R_{(f)} = \frac{R_{(\lambda, f)}}{R_{(\lambda, f_r)}}. \quad (\text{A.14.c})$$

In expressions (A.14),  $f_r$  is a convenient reference frequency. A specific guideline for choosing this reference frequency will be discussed later in this Appendix.

Then, taking the one dimensional Fourier transform of (A.13) and inserting (A.14.a) leads to:

$$V_{s(f)} = \int_0^{\infty} \Delta\phi_{(\lambda)} I_{(f)} R_{(\lambda)} R_{(f)} H_{ELECT(f)} d\lambda \text{ [volts/Hz]} \quad (\text{A.15})$$

which follows from the linearity property. Simplifying (A.15) produces:

$$V_{s(f)} = I_{(f)} R_{(f)} H_{ELECT(f)} \int_0^{\infty} \Delta\phi_{(\lambda)} R_{(\lambda)} d\lambda \text{ [volts/Hz]}. \quad (\text{A.16})$$

Therefore

$$v_{s(t)} = i'_{(t)} \int_0^{\infty} \Delta\phi_{(\lambda)} R_{(\lambda)} d\lambda \text{ [volts]}, \quad (\text{A.17})$$

where:

$$i'_{(t)} = i_{(t)} \star r_{(t)} \star h_{ELECT(t)}, \quad (\text{A.18})$$

and where  $r_{(t)}$  is the inverse transform of  $R_{(f)}$ .

Inherent to the definition of NETD is the concept of instantaneous signal-to-noise ratio which is represented as:

$$\frac{S}{N} = \frac{v_{s(t)}}{\sigma}, \quad (\text{A.19})$$

where  $\sigma$  is the rms noise voltage (A.7) and  $v_{s(t)}$  is the corresponding signal after the preamplifier. From (A.6) and (A.8):

$$\sigma = \left[ \int_0^{\infty} S'_{i(f)} H_{ELECT(f)}^2 df \right]^{\frac{1}{2}} \quad (\text{A.20})$$

and therefore,

$$\frac{S}{N} = \frac{i'_{(t)} \int_0^{\infty} \Delta\phi_{(\lambda)} R_{(\lambda)} d\lambda}{\left[ \int_0^{\infty} S'_{i(f)} H_{ELECT(f)}^2 df \right]^{\frac{1}{2}}} \quad (A.21)$$

Equation (A.21) provides the basis for the NETD calculation by setting the signal-to-noise ratio equal to one. However, it needs to be recast as a function of more standard parameters, including (obviously) the temperature difference between the target and background  $\Delta T$ .

The authors of the model included here a very reasonable assumption by taking  $i'_{(t)}=1$ . This is qualitatively explained by the fact that the normalized time function  $i_{(t)}$  must be equal to one at the midpoint of the signal (scanned target) where  $i'_{(t)}$  is measured. As represented on Figure A.2, for the horizontal scanning of the target, the duration of  $i_{(t)}$  is much greater than the response functions  $r_{(t)}$  and  $h_{ELECT(t)}$ . Therefore  $r_{(t)}$  and  $h_{ELECT(t)}$  are assumed to have approximately delta-function like behavior, which leads to the condition  $i'_{(t)}=1$ .

In order to recast (A.21), the concept of Spectral Noise Equivalent Power ( $NEP_{(\lambda)}$ ) must be introduced:

$$NEP_{(\lambda)} = \frac{\Delta\phi_{(\lambda)}}{\frac{V_{s(\lambda)}}{\sigma}} \text{ [watts]} \quad (A.22)$$

where:

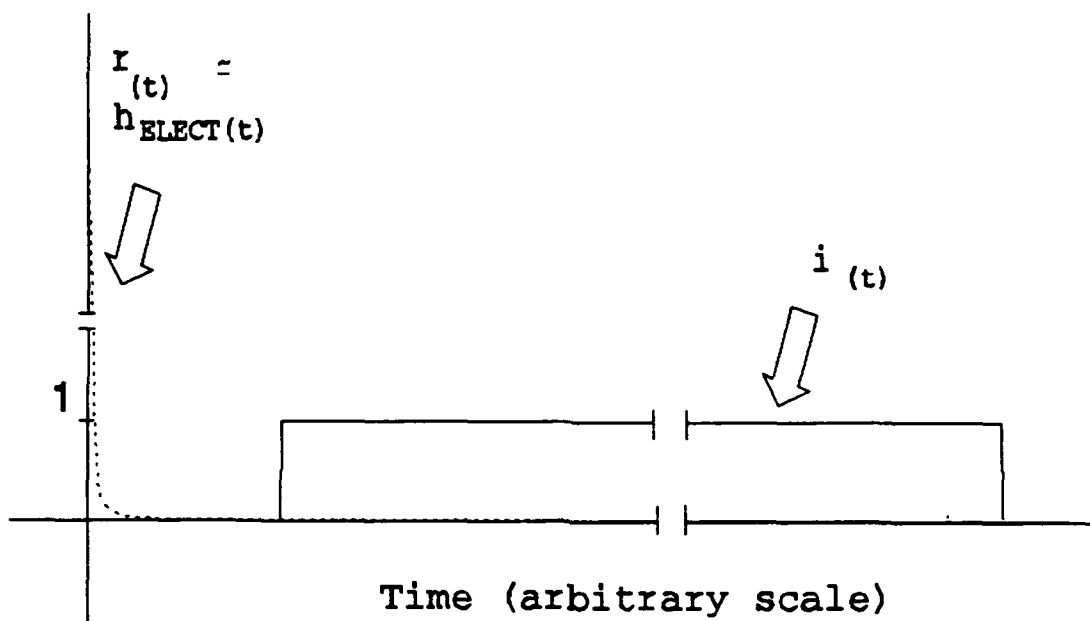


Figure A.2. Sample  $i_{(t)}$ ,  $r_{(t)}$ , and  $h_{ELECT(t)}$

$$V_{s(\lambda)} = \Delta\phi_{(\lambda)} R_{(\lambda)} \text{ [volts}/\mu\text{m}]. \quad (\text{A.23})$$

Note that since the NEP is defined for constant optical flux, the time dependence in this context has been dropped. Equation (A.22) implies a linear relation between the optical power and the resulting voltage signal, as shown in Figure A.3. The slope,  $R_{(\lambda)}$ , of this linear relation depends on wavelength. Definition (A.22) is in agreement with the more standard NEP definition in which a narrow band filter,  $\Delta\lambda$ , is employed [Ref. 34].

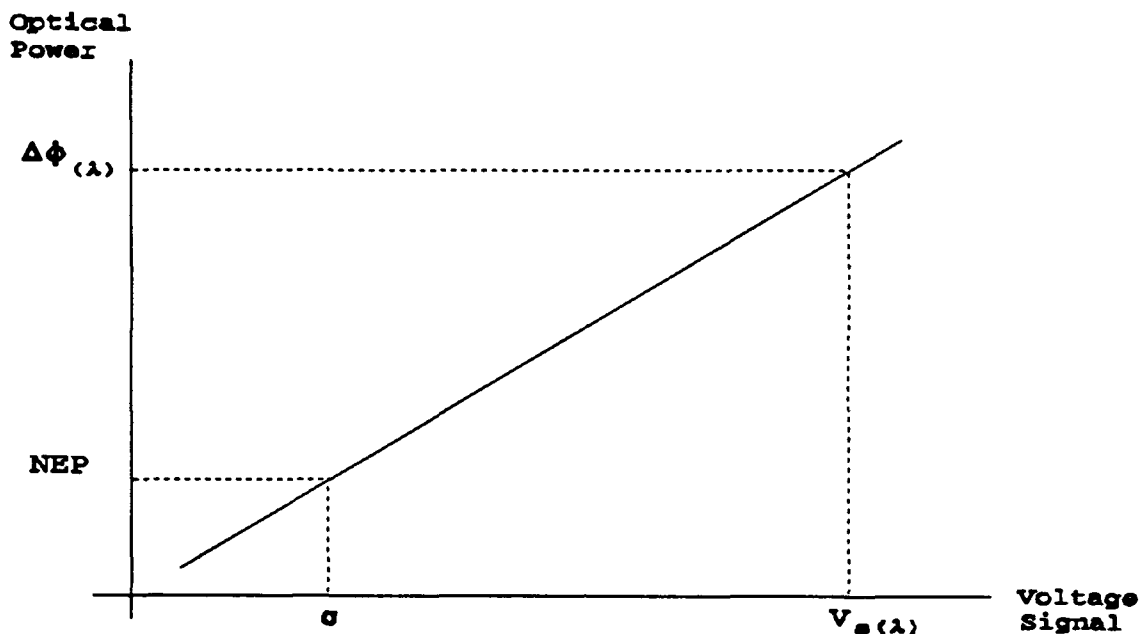


Figure A.3. Optical power versus Signal Voltage

A Spectral Specific Detectivity,  $D_{(\lambda)}^*$ , is defined as [Ref. 33, p. 270]:

$$D_{(\lambda)}^* \equiv \frac{(A_d \Delta f_n)^{\frac{1}{2}}}{NEP_{(\lambda)}} \left[ \frac{\text{cm Hz}^{\frac{1}{2}}}{\text{watts}} \right], \quad (\text{A.24})$$

where  $\Delta f_n$  is the noise equivalent electrical bandwidth (in Hz) of the circuitry considered in the noise measurement and  $A_d$  is the area of the detector [ $\text{cm}^2$ ]. If  $H_{\text{ELECT}(f)}$  represents the overall transfer function of the preamplifier-measurement device system, the noise bandwidth  $\Delta f_n$  is defined by [Ref. 30]:

$$\Delta f_n = \int_0^\infty \frac{S'_{i(f)}}{S'_{i(f_r)}} H_{\text{ELECT}(f)}^2 df \quad (\text{A.25})$$

such that by direct comparison with (A.20):

$$\sigma = S'_{i(f_r)} \Delta f_n. \quad (\text{A.26})$$

Therefore, after substituting (A.22), (A.23), and (A.26) into (A.24), it is found that:

$$D_{(\lambda)}^* = \frac{A_d^{\frac{1}{2}} R_{(\lambda)}}{(S'_{i(f_r)})^{\frac{1}{2}}}. \quad (\text{A.27})$$

This leads to a new expression for the signal-to-noise ratio:

$$\frac{S}{N} = \frac{\int_0^\infty \Delta \phi_{(\lambda)} D_{(\lambda)}^* d\lambda}{[A_d \int_0^\infty \frac{S'_{i(f)}}{S'_{i(f_r)}} H_{\text{ELECT}(f)}^2 df]^{\frac{1}{2}}} = \frac{\int_0^\infty \Delta \phi_{(\lambda)} D_{(\lambda)}^* d\lambda}{[A_d \Delta f_n]^{\frac{1}{2}}}. \quad (\text{A.28})$$

Next, the model assumes for a simple imaging system:

$$\Delta \phi_{(\lambda)} = \frac{\pi A_d}{4 F^2} \eta_{o(\lambda)} \frac{\partial L_{(\lambda)}}{\partial T} \Delta T \quad (\text{A.29})$$

where:

$\eta_{o(\lambda)}$  = Optical efficiency of the viewer,

$F$  = f/number = focal length (d)/diameter of the  
aperture stop (D) [Ref. 33, p. 179],

$T$  = Temperature,

$L_{(\lambda)}$  = Spectral Radiance [watts/(cm<sup>2</sup> steradian μm)] from  
the source.



This follows after noting that the approximate solid angle subtended by the lens (with respect to its focal point) is:

$$\Omega_{\text{lens}} = \frac{\pi \left( \frac{D}{2} \right)^2}{d^2} = \frac{\pi}{4F^2} .$$

The expression (A.29) describes the focusing process performed by the lens and the subsequent collection of the energy focused onto the focal plane by each detector. It also implies that the spectral irradiance onto the detector  $H_{(\lambda)}$  is:

$$H_{(\lambda)} = \frac{\Delta\phi_{(\lambda)}}{A_d} = \frac{\pi}{4F^2} \eta_{0(\lambda)} \frac{\partial L_{(\lambda)}}{\partial T} \Delta T \text{ [watts/(cm}^2 \text{ }\mu\text{m)}]}. \quad (\text{A.30})$$

Finally, after substituting (A.29) into (A.28):

$$\frac{S}{N} = \frac{\pi A_d^{\frac{1}{2}} \Delta T \int_0^\infty \eta_{0(\lambda)} \frac{\partial L_{(\lambda)}}{\partial T} D_{(\lambda)}^* d\lambda}{4F^2 (\Delta f_n)^{\frac{1}{2}}}. \quad (\text{A.31})$$

By setting the signal-to-noise ratio equal to one,  $\Delta T$  becomes the NETD:

$$\text{NETD} = \frac{4F^2 (\Delta f_n)^{\frac{1}{2}}}{\pi A_d^{\frac{1}{2}} \int_0^\infty \eta_{0(\lambda)} \frac{\partial L_{(\lambda)}}{\partial T} D_{(\lambda)}^* d\lambda} \text{ [}^\circ\text{C]}. \quad (\text{A.32})$$

There is one additional condition. By convention the NETD parameter assumes the use of an external measurement filter. In essence this restricts the measured signal-to-noise ratio

to be dependent on parameters such as the detector angular subtense (DAS), but not the bandlimiting components making up the TIS. The external filter should be designed such that the overall MTF will satisfy:

$$H_{\text{ELECT}}^2(f) = \frac{1}{1 + \left(\frac{f}{f_r}\right)^2} \quad (\text{A.33.a})$$

where the 3-dB power bandwidth meets the condition:

$$f_r = \frac{1}{2\tau_d} \quad (\text{A.33.b})$$

where  $\tau_d$  is the detector dwell time. It follows from the definition (A.25) and the white noise condition,  $S_i'_{(f)}/S_i'_{(fr)}=1$ , that:

$$\Delta f_n = f_r \frac{\pi}{2} \quad (\text{A.33.c})$$

which was determined through use of a convenient table of integrals [Ref. 35]. For consistent comparison of NETD associated with thermal imaging systems the noise bandwidth should satisfy (A.33.c).

For a single detector system, with 100% scanning efficiency, the dwell time is given by:

$$\tau_d = \frac{1}{F_r} \frac{\Delta x \Delta y}{(\text{HFOV})(\text{VFOV})} \quad (\text{A.34})$$

which follows from the geometry shown in Figure I.4. Extending this result to cover non-unity scanning efficiency and

overscan ratio as well as systems based on a parallel detection scheme, leads to:

$$f_r = \frac{1}{2\tau_d} = \frac{(HFOV)(VFOV)F_r\eta_{ovsc}}{2n_p\Delta x\Delta y\eta_{sc}} \text{ [Hz]} \quad (\text{A.35})$$

where:

HFOV = device horizontal field of view [mrad]

VFOV = device vertical field of view [mrad]

$F_r$  = frame rate [Hz]

$\eta_{ovsc}$  = overscan ratio for the device

$n_p$  = number of detectors in parallel

$\Delta x$  = horizontal detector size [mrad]

$\Delta y$  = vertical detector size [mrad]

$\eta_{sc}$  = scan efficiency (fraction of time spent in actually scanning the field), and

$\tau_d$  = dwell time (time the detector takes to scan a picture element  $\Delta x\Delta y$ ) [sec].

Again, it is important to remember that the actual system noise bandwidth is the one stated in (A.25), and that the approximation given in (A.33.c) is only valid if the measuring device, which includes  $H^2_{ELECT(f)}$ , is adjusted so that the true bandwidth of (A.25) equals the standardized one of (A.33.c). A demonstrative plot of  $\Delta f_n$  and  $H^2_{ELECT(f)}$  for the sample system employed in this thesis is presented in Figure A.4. The physical interpretation is that the area under the curve is equal to  $\Delta f_n$ .

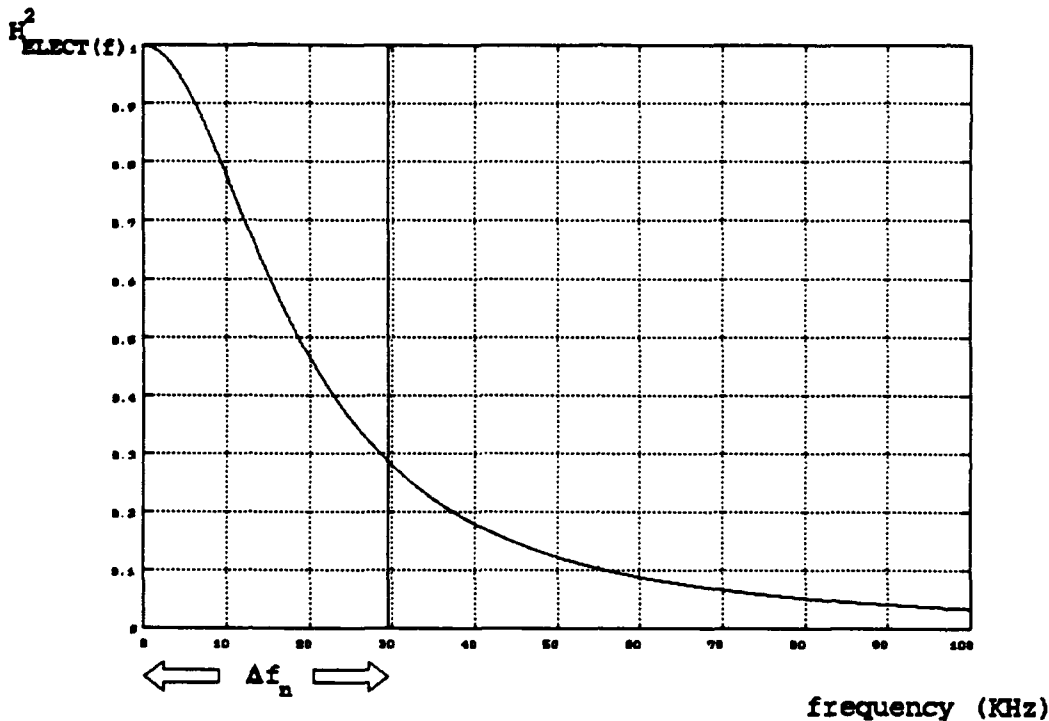


Figure A.4. Noise equivalent bandwidth ( $\Delta f_n$ ) and  $H^2_{ELECT}(f)$

A standard approximation which is usually used to simplify (A.32) is introduced in Chapter II, Section A.

#### C. DERIVATION OF THE MINIMUM RESOLVABLE TEMPERATURE DIFFERENCE (MRTD)

The standard target with which the MRTD has historically been measured and modeled consists of four bars in which the height (L) is equal to seven times their width (W), equally spaced by a distance W. The derivation for the MRTD that follows considers this standard pattern and assumes no sampling effects along the direction of scanning. Probably

the most important assumption of this derivation is the representation of the perceptual recognition process that takes place in the eye-brain system by means of a matched filter.

For a viewed object (the image obtained from the system) characterized by the dimensionless spatial function  $i_{(x,y)}$ , such a matched filter would have a response function:

$$h_{mf(x,y)} = K i_{(-x,-y)} \quad (\text{A.36})$$

where  $K$  is a constant that can for convenience be set equal to one, but will carry the standard units for a 2D space domain matched filter [ $\text{angle}^{-2}$ ].

From the space domain version of (A.6), the output rms noise from that matched filter would be:

$$N_{mf} = \left[ \int_{-\infty}^{\infty} \int_{-\infty}^{\infty} S_{(f_x, f_y)} H_{mf}^2(f_x, f_y) df_x df_y \right]^{\frac{1}{2}} \quad (\text{A.37.a})$$

where  $H_{mf}$  is the Fourier transform of the matched filter impulse response (A.36). It follows that:

$$N_{mf} = K \left[ \int_{-\infty}^{\infty} \int_{-\infty}^{\infty} S_{(f_x, f_y)} I_{(f_x, f_y)}^2 df_x df_y \right]^{\frac{1}{2}} . \quad (\text{A.37.b})$$

where  $S_{(f_x, f_y)}$  is now the double-sided PSD of the observed noise and  $I_{(f_x, f_y)}$  is the 2D spatial Fourier transform of  $i_{(x,y)}$ .

Mainly because of the MTF degradations that must be considered, the authors explain the computational advantage of assuming the matched filter as one established for a "(potentially) infinite periodic pattern".

In the direction of scanning (x) the matched filter is defined as an undegraded rect function of width equal to the width of the bars. In the other direction (y) it is just the degraded rect function of width equal to the length of the bars. This can be explained by thinking of the human eye-brain system as one prepared to recognize four vertical bars. The horizontal direction being critical, the observer expects sharp edges along x (regardless of the sharpness in y) to accomplish the recognition process. Figure A.5 shows this concept.

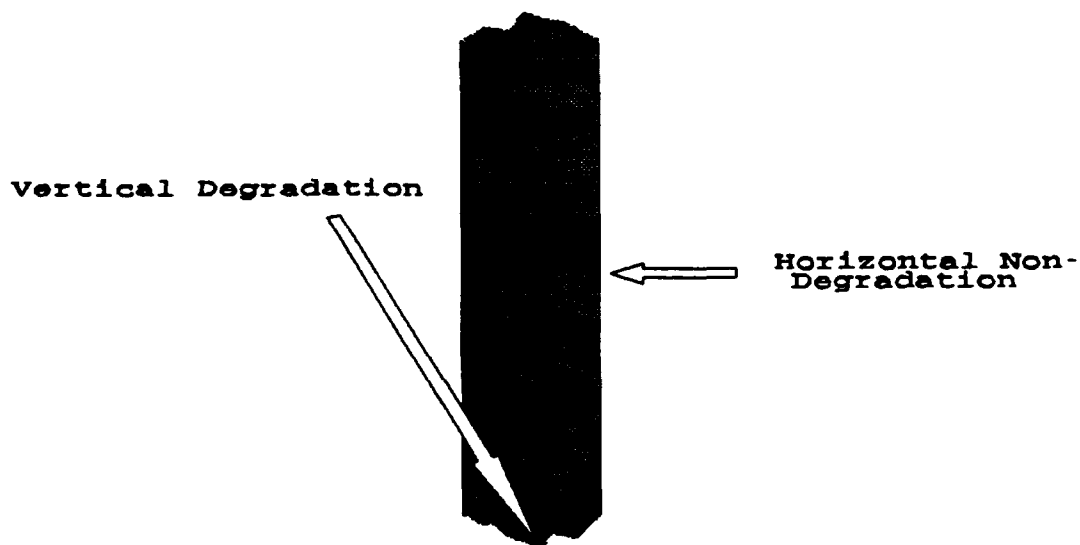


Figure A.5. Ratches matched filter

Because both signal and noise are passed through the same matched filter the choice to use a single bar representation is only one of mathematical convenience.

To perform the MRTD derivation, Ratches et al. started by defining the signal energy per unit angular area of the display as:

$$M_{(x,y)} = \frac{k \Delta T i_{(x,y)}}{\Delta y_i v_x} \left[ \frac{\text{Joules}}{\text{mrad}^2} \right], \quad (\text{A.38})$$

where:

$k\Delta T$  = watts emitted by a display element for a large target with a temperature difference  $\Delta T$  with respect to background,

$\Delta y_i$  = angular distance between scan lines ( $\Delta y / \eta_{ovsc}$ ),

$v_x$  = angular scan velocity of display element ( $\Delta x / \tau_d$ ),

$i_{(x,y)}$  = spatial distribution of viewed object

=  $i_{T(x,y)} * h_{D(x,y)}$ ,

$\tau_d$  = dwell time,

$i_{T(x,y)}$  = spatial distribution of the original target, and

$h_{D(x,y)}$  = system response function.

Equation (A.38) provides a useful rule for conversion between temperature and energy units. Proportionality with  $\Delta T$  reflects the AC coupling inherent in most FLIR systems.

Formally expressed, the assumed periodic target  $i_{T(x,y)}$  results:

$$i_{T(x,y)} = \text{sgn}(\sin(2\pi f_{ox}x)) i_{T(y)}. \quad (\text{A.39})$$

where  $f_{ox}$  is the horizontal spatial frequency of the target measured in cycles/mrad. This implies that the function  $i_{T(x,y)}$  can be separated into two independent functions along each

dimension such that  $i_{T(x,y)} = i_{T(x)} i_{T(y)}$ . Figure A.6 depicts a sample  $i_{T(x)}$ .

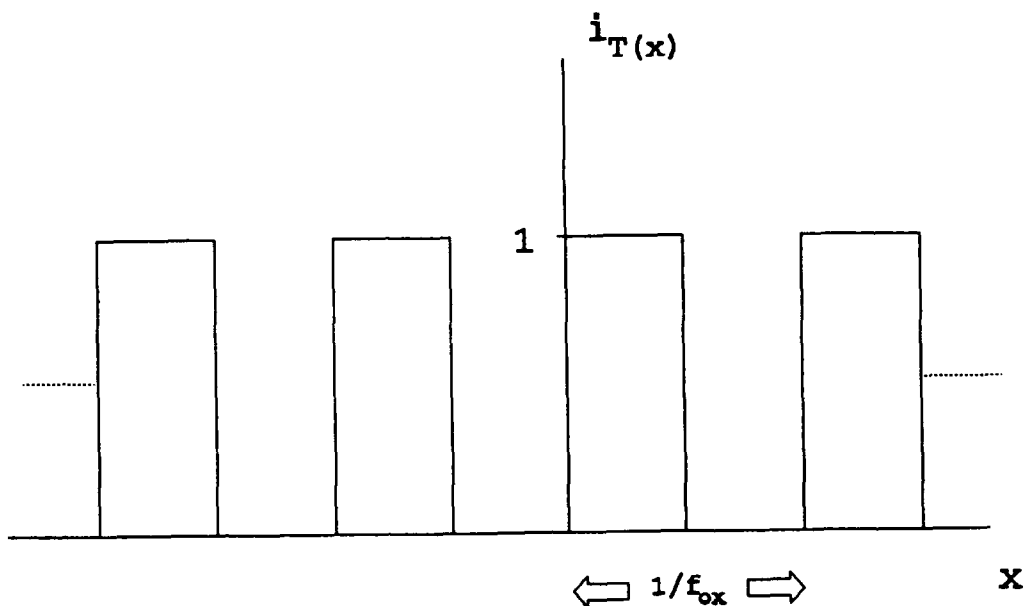


Figure A.6. Sample  $i_{T(x)}$

The periodic model for the target is acceptable if the output signal is seen as the difference between the energy of the target passed a) through the matched filter centered over the target and b) through the matched filter centered over the background.

Applying (A.38), and the concept of periodic matched filter, the signal used in the MRTD calculation will be:



$$S = \text{Max} \left[ \frac{k \Delta T}{\Delta y_i v_x} i_{(x,y)} \star h_{mf(x,y)} \right] - \text{Min} \left[ \frac{k \Delta T}{\Delta y_i v_x} i_{(x,y)} \star h_{mf(x,y)} \right] \left[ \frac{\text{Joules}}{\text{mrad}^2} \right] \quad (\text{A.40})$$

representing the dynamic range in the energy signal.

In order to simplify the derivation, the model assumes that the function  $i_{(x,y)}$  can be approximated horizontally by using the first two terms of the series expansion of  $i_{I(x)}$ . The resulting sine expansion chosen by the authors corresponds to an odd  $i_{I(x)}$ . An even function is used in Appendix C which is consistent with a centered target in the object plane. This difference is not relevant for the final result. Thus:

$$i_{(x,y)} = [0.5 + H_{D(f_{ox})} \frac{2}{\pi} \sin(2\pi f_{ox} x)] i_{(y)} \quad (\text{A.41})$$

where  $i_{(y)}$  is the degraded vertical function that corresponds to the length of the target. Therefore, substituting (A.41) into (A.40) leads to:

$$S = 2 \frac{k \Delta T}{\Delta y_i v_x} \frac{2}{\pi} H_{D(f_{ox})} \int_0^{2f_{ox}} \sin(2\pi f_{ox} x) (2f_{ox}) dx \int_{-\infty}^{\infty} I_{(f_y)} H_{mf(f_y)} df_y \left[ \frac{\text{Joules}}{\text{mrad}^2} \right] \quad (\text{A.42})$$

In the calculation of (A.42) the DC term in (A.41) canceled out. Both Min[] and Max[] terms in (A.40) contribute equally. As discussed in Chapter IV, the replacement of the full periodic spectrum by the first two terms turns out to be an extremely good approximation for the sample system specified in Appendix D.

In equation (A.42), the horizontal integral is evaluated in space and the vertical in spatial frequency. The first integral uses a matched filter of width  $1/(2f_{ox})$  and an amplitude of  $2f_{ox}$  under the convention of a normalized area of one ( $H_{(f_x)}=1$  for  $f_x=0$ ). The first integral equals  $2/\pi$  and the second one can be simplified since:

$$H_{mf(f_y)} = H_{T(f_y)} H_{D(f_y)} \quad (\text{A.43.a})$$

and

$$I(f_y) = L H_{T(f_y)} H_{D(f_y)} \quad (\text{A.43.b})$$

where:

$L$  = length of a bar [mrad],

$H_{T(f_y)}$  = normalized transform of the target along the y direction (see (C.11)), and

$H_{D(f_y)}$  = normalized transfer function of the overall system along the y direction.

Finally the expression for signal considered for MRTD can be recast to:

$$S = \frac{k \Delta T L}{\Delta Y_i v_x} \frac{8}{\pi^2} H_{D(f_{ox})} \int_{-\infty}^{\infty} H_{T(f_y)}^2 H_{D(f_y)}^2 df_y \left[ \frac{\text{Joules}}{\text{mrad}^2} \right] \quad (\text{A.44})$$

With respect to the noise analysis that will be used, the model starts by recognizing the need to produce an expression for the power spectrum of the displayed noise. The noise on the display is given by the following equation:

$$n_{(x,y)} = \sum_i b_{i(x)} \delta_{(y-y_i)} * h_{d(y)} = \sum_i b_{i(x)} h_{d(y-y_i)} \left[ \frac{\text{Joules}}{\text{mrad}^2} \right] \quad (\text{A.45})$$

where  $h_{d(y)}$  is the impulse response of the display in the  $y$  direction. The function  $b_{i(x)}$  is related to a voltage noise function, along the  $i^{\text{th}}$  video line, which has been converted to a one-dimensional radiant function by the display, and the spread produced on each line of the monitor (represented by the convolution). Therefore,  $n_{(x,y)}$  includes the noise contribution of all the scanning lines on every single point of the display. The autocorrelation of  $n_{(x,y)}$  is:

$$\begin{aligned} \langle n_{(x,y)} n_{(x_\tau, y_\tau)} \rangle &= \left\langle \sum_i b_{i(x)} b_{j(x_\tau)} h_{d(y-y_i)} h_{d(y_\tau-y_j)} \right\rangle \\ &= \sum_i \sum_j \langle b_{i(x)} b_{j(x_\tau)} \rangle h_{d(y-y_i)} h_{d(y_\tau-y_j)} \left[ \frac{\text{Joules}}{\text{mrad}^2} \right]^2 \end{aligned} \quad (\text{A.46})$$

since  $\langle [] \rangle$  represents averaging along the  $x$  direction, where the random process takes place.

Ratches et al. assume a noise with mean equal to zero ( $\langle b_{i(x)} \rangle = 0$ ). Then the result of  $\langle b_{i(x)} b_{j(x_\tau)} \rangle$  equals zero for all values of  $i$  and  $j$  except for  $i=j$  since  $b_i$  and  $b_j$  are independent random processes, except for the case  $i=j$ . Then, the autocorrelation becomes:

$$R_{(xx_\tau yy_\tau)} = \langle n_{(x,y)} n_{(x_\tau, y_\tau)} \rangle = \sum_i \langle b_{i(x)} b_{i(x_\tau)} \rangle h_{d(y-y_i)} h_{d(y_\tau-y_i)} \quad (\text{A.47})$$

Assuming all the video lines are statistically equivalent,  $\langle b_{i(x)} b_{i(x_\tau)} \rangle$  is independent of  $i$ , and therefore:

$$R_{(xx,yy)} = \langle b_{(x)} b_{(x_r)} \rangle \sum_i h_{d(y-y_i)} h_{d(y_r-y_i)} \quad (\text{A.48})$$

After approximating (A.48) by an integral (i.e., the sampling artifacts of the display are being ignored), the resulting form is:

$$R_{(xx,yy)} = \langle b_{(x)} b_{(x_r)} \rangle \frac{1}{\Delta y_i} \int_{-\infty}^{\infty} h_{d(y-y_i)} h_{d(y_r-y_i)} dy_i \quad (\text{A.49})$$

where  $\Delta y_i$  is the angular spread between adjacent vertical video lines.

This equation can be recast by using the appropriate change of variables:

$$p = y_r - y_i$$

$$y = y - y_r$$

$$x = x - x_r$$

Assuming the process in  $x$  is wide-sense stationary ( $\langle b_{(x)} b_{(x_r)} \rangle$  depends only upon  $x - x_r$ ):

$$R_{(xy)} = R_{(xx,yy)} = \langle b_{(x)} b_{(x_r)} \rangle \frac{1}{\Delta y_i} \int_{-\infty}^{\infty} h_{d(p)} h_{d(y+p)} dp \quad (\text{A.50})$$

Then, to obtain the power spectrum of the noise, the Fourier transform of  $R_{(xy)}$  is performed:

$$S_{(f_x, f_y)} = \int_{-\infty}^{\infty} \langle b_{(x)} b_{(x_r)} \rangle e^{-j2\pi f_x x} dx \frac{1}{\Delta y_i} H_{d(f_y)} H_{d(f_y)}^* \left[ \frac{\text{Joules}^2}{\text{mrad}^2} \right] \quad (\text{A.51})$$

after use of the Correlation theorem [Ref. 39]. The Fourier transform of  $\langle b_{(x)} b_{(x_r)} \rangle$  generates the voltage noise PSD (prior to the display) " provided the units are properly transformed

from 'voltage' and 'voltage' space to radiant energy and display space [Ref. 30]". In other words,  $S_{(f_x, f_y)}$  is the displayed noise PSD and it is expressed in radiant energy units/mrad. Assuming  $S_{(f_x, f_y)} = S_{(f_x)} S_{(f_y)}$ , where:

$$S_{(f_x)} = \int_{-\infty}^{\infty} \langle b_{(x)} b_{(x_\tau)} \rangle e^{-j2\pi f_x x} dx \left[ \frac{\text{Joules}^2}{\text{mrad}} \right] \quad (\text{A.52.a})$$

$$S_{(f_y)} = \frac{1}{\Delta y_i} H_{d(f_y)} H_{d(f_y)}^* \left[ \frac{1}{\text{mrad}} \right]. \quad (\text{A.52.b})$$

Noting that there is a linear relation between voltage and radiant energy,  $S_{(f_x)}$  can be reinterpreted as an electrical, optical or thermal noise PSD provided the appropriate unit conversion is performed to leave  $S_{(f_x, f_y)}$  unchanged. Applying (A.6):

$$S_{o(f_x)} = S_{i(f_x)} H_{\text{ELECT}}^2(f_x) \quad (\text{A.53.a})$$

or

$$S_{o(f_x)} = \Gamma \frac{S_{i(f_x)}}{S_{i(f_{rx})}} H_{\text{ELECT}}^2(f_x) [\text{power}_{\text{temp units mrad}}] \quad (\text{A.53.b})$$

where  $\Gamma$  is a constant such that the expression can be referred to temperature units instead of volts. This is performed in order to make the units of the noise compatible with those of the signal. In the next paragraph it is shown that the correct power temperature units is  $(^\circ\text{C})^2$ .

To determine the value of this constant  $\Gamma$ , the concept from (A.19) can be used. If both signal and noise are

expressed in temperature units, by setting  $S/N=1$ , the signal (NETD by definition) is equal to the rms noise voltage, and, since  $f$  (temporal frequency)  $= v_x$  (scanning velocity)  $\cdot f_x$  (spatial frequency in  $x$ ), (A.20) can be recast to:

$$\text{NETD} = \sigma = \left[ \int_0^\infty \Gamma \frac{S'_{i(f_x)}}{S'_{i(f_{rx})}} H_{\text{ELECT}}^2(f_x) df_x \right]^{\frac{1}{2}} = [\Gamma \Delta f_{xn}]^{\frac{1}{2}} = \left[ \frac{\Gamma \Delta f_n}{v_x} \right]^{\frac{1}{2}} [^\circ\text{C}] \quad (\text{A.54})$$

where  $\Delta f_{xn}$  is the noise bandwidth defined in terms of spatial frequencies. Using the more commonly seen reference bandwidth in Hz, the constant  $\Gamma$  becomes:

$$\Gamma = \frac{\text{NETD}^2 v_x}{\Delta f_n} [^\circ\text{C}^2 \text{ mrad}] \quad (\text{A.55})$$

Then, the noise power spectral density (A.52.a) in  $x$  can be represented by:

$$\int_{-\infty}^{\infty} \langle b_{(x)} b_{(x_r)} \rangle e^{j2\pi f_x x} dx \rightarrow \text{NETD}^2 \frac{1}{\Delta f_n} v_x \frac{S_{i(f_x)}}{S_{i(f_{rx})}} H_{\text{ELECT}}^2(f_x) [^\circ\text{C}^2 \text{ mrad}] \quad (\text{A.56})$$

where the arrow indicates an allowed substitution after converting from voltage to thermal units.

Since an expression for the **displayed** noise power spectrum is expected, the temperature value of the NETD must be converted into radiant energy, following a similar approach as in (A.38). Then:

$$\text{NETD}' \leftrightarrow k \frac{\text{NETD}}{v_x} [\text{Joules/mrad}] \quad (\text{A.57})$$

and after substitution of  $\text{NETD}'$  for NETD in (A.56)

$$\int_{-\infty}^{\infty} \langle b_{(x)} b_{(x_r)} \rangle e^{j2\pi f_x x} dx \rightarrow \frac{k^2 \text{NETD}^2}{v_x \Delta f_n} \frac{S_{i(f_x)}}{S_{i(f_{rx})}} H_{\text{ELECT}(f_x)}^2 \left[ \frac{\text{Joules}^2}{\text{mrad}} \right]. \quad (\text{A.58})$$

Thus, recombining (A.51), and including the display transfer function along  $x$  ( $H_{d(f_x)}$ ):

$$S_{(f_x, f_y)} = \frac{k^2 \text{NETD}^2}{v_x \Delta y_i \Delta f_n} \frac{S_{i(f_x)}}{S_{i(f_{rx})}} H_{\text{ELECT}(f_x)}^2 H_{d(f_x, f_y)}^2 \left[ \frac{\text{Joules}^2}{\text{mrad}^2} \right]. \quad (\text{A.59})$$

As previously stipulated, expression (A.59) for the displayed noise spectral density has the same dimensions as (A.51). From (A.10) the matched filter can be defined as:

$$H_{mf(f_x, f_y)} = (H_{w(f_x)} H_{T(f_y)} H_{D(f_y)})^* \quad (\text{A.60})$$

where  $H_{w(f_x)}$  is the normalized undegraded Fourier transform of one bar along  $x$  (See Appendix C). After substitution of (A.59) and (A.60) into (A.37.a), the matched-filter noise (perceived noise) results:

$$N_{mf} = \left[ \frac{k^2 \text{NETD}^2}{v_x \Delta y_i \Delta f_n} \int_{-\infty}^{\infty} \int_0^{\infty} \frac{S'_{i(f_x)}}{S'_{i(f_{rx})}} H_{\text{ELECT}(f_x)}^2 H_{d(f_x, f_y)}^2 H_{w(f_x)}^2 H_{T(f_y)}^2 H_{D(f_y)}^2 df_x df_y \right]^{\frac{1}{2}} \quad (\text{A.61})$$

[Joules/mrad<sup>2</sup>].

It is noted that, as required by the S/N calculation to be discussed in the next paragraph, (A.61) and (A.44) are dimensionally consistent.

Finally, the expression for the MRTD results from combining (A.44) with (A.61) and solving for  $\Delta T$  with a threshold value of signal-to-noise ratio  $\Psi$ . An improvement factor of  $F_r \cdot t_e$

(frame rate x eye integration time) is applied to the signal since it is assumed a process of summation of the signal and noise over the frames in an eye integration time. Thus, the MRTD expression obtained is:

MRTD

$$= \frac{\Delta y_i v_x \frac{\pi^2}{8} \Psi}{H_{D(f_{ox})} L \int_{-\infty}^{\infty} H_T^2(f_y) H_D^2(f_y) df_y} \cdot \left[ \frac{NETD^2}{v_x \Delta y_i \Delta f_n F_r t_e} \int_{-\infty}^{\infty} \int_0^{\infty} \frac{S'_i(f_x)}{S'_i(f_{rx})} H_{ELECT}^2(f_x) H_d^2(f_x, f_y) H_w^2(f_x) H_T^2(f_y) H_D^2(f_y) df_x df_y \right]^{\frac{1}{2}}$$

or

$$= \frac{\frac{\pi^2}{8} \Psi NETD}{H_{D(f_{ox})} L \int_{-\infty}^{\infty} H_T^2(f_y) H_D^2(f_y) df_y} \cdot \left[ \frac{v_x \Delta y_i}{\Delta f_n F_r t_e} \int_{-\infty}^{\infty} \int_0^{\infty} \frac{S'_i(f_x)}{S'_i(f_{rx})} H_{ELECT}^2(f_x) H_d^2(f_x, f_y) H_w^2(f_x) H_T^2(f_y) H_D^2(f_y) df_x df_y \right]^{\frac{1}{2}} \quad (A.62)$$

Expression (A.62) may be somewhat misleading since an ostensible dependency of the MRTD on the frame rate ( $F_r$ ) shows up.

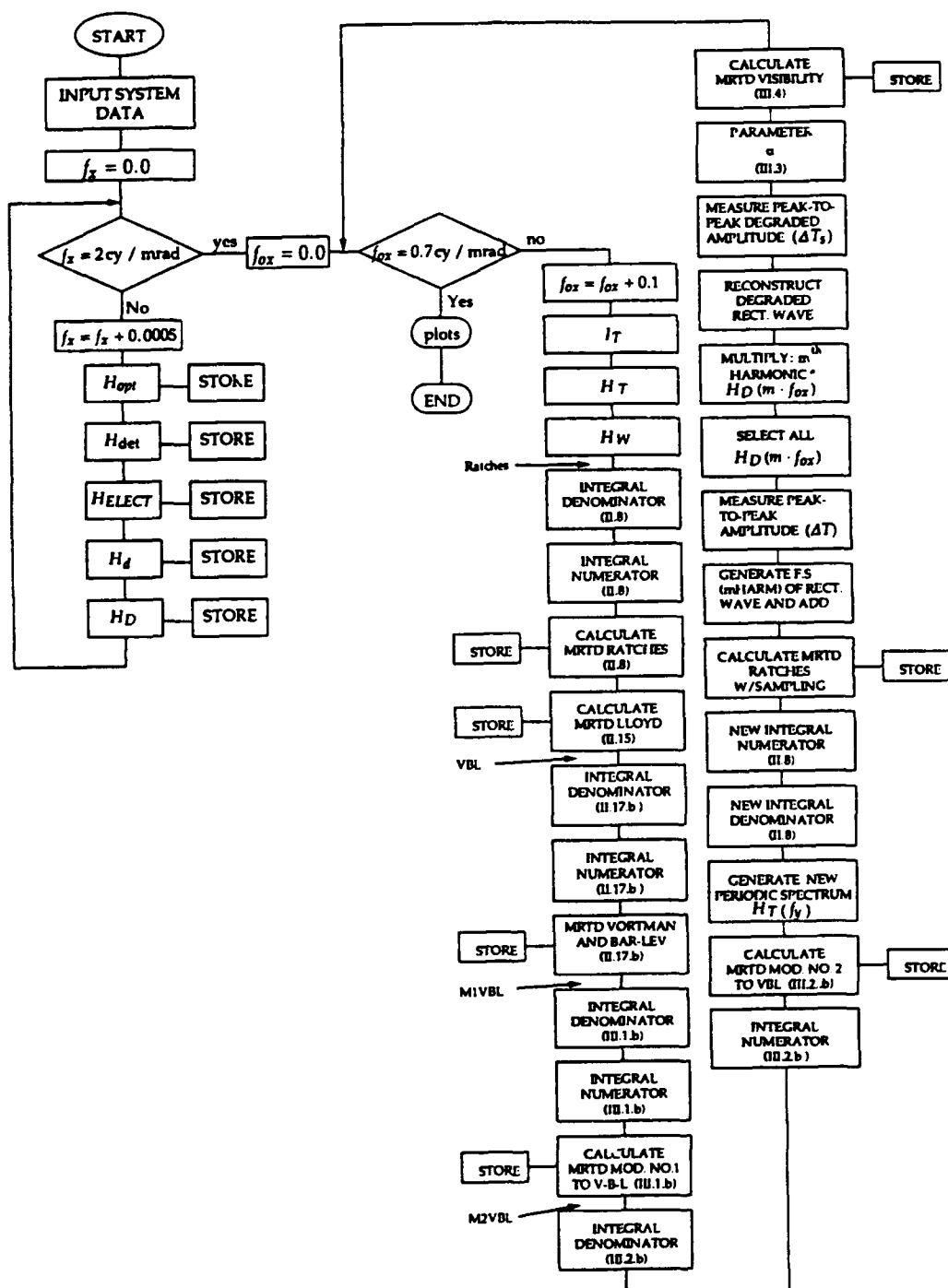
However, the NETD has a similar dependence on the same parameter (equations (A.32) and (A.33)) and the overall effect cancels out. As pointed out by Lloyd's observations [Ref. 10, p.189], the MRTD does not depend on the frame rate.

It is worth noting that, in the limit  $f_{ox} \rightarrow 0$  [cy/mrad], the MRTD is actually lower, i.e., more optimistic, than the NETD (A.32). This is qualitatively explained by the intro-



duction of an eye-brain matched filter. It has been determined that the improvement factor for the sample system (Appendix D) is approximately 1.58. See Chapter III, Section B.

## APPENDIX B - DESCRIPTIVE FLOWCHART OF SIMULATION



## APPENDIX C - EXACT FOUR-BAR FOURIER SPECTRUM

The standard 4-bar pattern and the coordinates considered in this work are shown in the Figure C.1 :

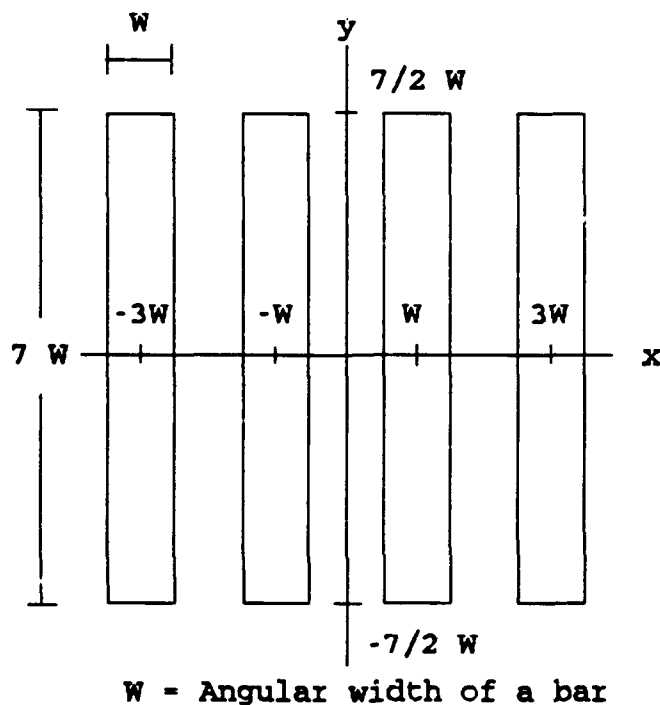


Figure C.1. MRTD Standard target

The bar pattern can be represented by the following two-dimensional function:

$$i_T(x,y) = \left[ \text{Rect} \left( \frac{x-W}{W} \right) + \text{Rect} \left( \frac{x+W}{W} \right) + \text{Rect} \left( \frac{x-3W}{W} \right) + \text{Rect} \left( \frac{x+3W}{W} \right) \right] \text{Rect} \left( \frac{y}{7W} \right) \quad (\text{C.1})$$

The two-dimensional Fourier transform is defined as follows:

$$\mathcal{F}_{2D} \{ i_{T(x,y)} \} = \int_{-\infty}^{\infty} \int_{-\infty}^{\infty} i_{T(x,y)} e^{-j(k_x \cdot x + k_y \cdot y)} dx dy \quad (C.2)$$

where  $k_x = 2\pi f_x$  and  $k_y = 2\pi f_y$ . Both spatial frequencies,  $f_x$  and  $f_y$ , are expressed in cycles/mrad.

Since this two-dimensional function can be separated in two independent factors such that  $i_{T(x,y)} = i_{T(x)} i_{T(y)}$ , the two-dimensional Fourier transform can be expressed as:

$$\mathcal{F}_{2D} \{ i_{T(x,y)} \} = \mathcal{F}_{1D} \{ i_{T(x)} \} \mathcal{F}_{1D} \{ i_{T(y)} \} \quad (C.3)$$

Then:

$$\mathcal{F}_{1D} \left\{ \text{Rect} \left( \frac{x}{W} \right) \right\} = \int_{-\frac{W}{2}}^{\frac{W}{2}} e^{-j(k_x \cdot x)} dx = \frac{2}{k_x} \sin(k_x \frac{W}{2}) \quad (C.4)$$

Applying Shifting theorem for the four bars of the target:

$$\mathcal{F}_{1D} \{ i_{T(x)} \} = \frac{2}{k_x} \sin(k_x \frac{W}{2}) [e^{-jk_x W} + e^{jk_x W} + e^{-j3k_x W} + e^{j3k_x W}] \quad (C.5)$$

$$= \frac{2}{k_x} [-\sin(k_x \frac{W}{2}) + \sin(3k_x \frac{W}{2}) - \sin(5k_x \frac{W}{2}) + \sin(7k_x \frac{W}{2})] \quad (C.6)$$

$$= W [-\text{Sa}(k_x \frac{W}{2}) + 3\text{Sa}(3k_x \frac{W}{2}) - 5\text{Sa}(5k_x \frac{W}{2}) + 7\text{Sa}(7k_x \frac{W}{2})] \quad (C.7)$$

where  $\text{Sa}(u) = \sin(u)/u$ . Similarly, in the y-dimension:

$$\begin{aligned} \mathcal{F}_{1D} \{ i_{T(y)} \} &= \int_{-7\frac{W}{2}}^{7\frac{W}{2}} e^{-j(k_y y)} dy = \frac{2}{k_y} \sin(7k_y \frac{W}{2}) \\ &= 7 W \text{Sa}(7k_y \frac{W}{2}) \end{aligned} \quad (\text{C.8})$$

Finally, the two-dimensional Fourier transform of the standard 4-bar pattern results:

$$\begin{aligned} \mathcal{F}_{2D} \{ i_{T(x,y)} \} &= 7W^2 [ -\text{Sa}(k_x \frac{W}{2}) + 3\text{Sa}(3k_x \frac{W}{2}) - \\ &\quad 5\text{Sa}(5k_x \frac{W}{2}) + 7\text{Sa}(7k_x \frac{W}{2}) ] \text{Sa}(7k_y \frac{W}{2}) \end{aligned} \quad (\text{C.9})$$

or expressed as a function of  $f_x, f_y$ :

$$\begin{aligned} I_{T(f_x, f_y)} = \mathcal{F}_{2D} \{ i_{T(x,y)} \} &= 7W^2 [ -\text{Sa}(\pi f_x W) + 3\text{Sa}(3\pi f_x W) - \\ &\quad 5\text{Sa}(5\pi f_x W) + 7\text{Sa}(7\pi f_x W) ] \text{Sa}(7\pi f_y W) \end{aligned} \quad (\text{C.10})$$

which is coincident with the expression employed by J.G. Vortman and A. Bar-Lev in the model discussed in Chapter II [Ref. 8].

The target spectrum is normalized to obtain the unitless  $H_{T(f_y)}$ ,  $H_{T(f_x)}$ , and  $H_{W(f_x)}$  employed in the Ratches [Ref. 5] and Vortman and Bar-Lev models [Ref. 8]. Thus:

$$H_{T(f_y)} = \frac{I_{T(f_y)}}{7 W} = \text{Sa}(7k_y \frac{W}{2}), \quad (\text{C.11})$$

$$\begin{aligned} H_{T(f_x)} = \frac{I_{T(f_x)}}{4 W} &= \frac{1}{4} [ -\text{Sa}(k_x \frac{W}{2}) + 3\text{Sa}(3k_x \frac{W}{2}) - \\ &\quad 5\text{Sa}(5k_x \frac{W}{2}) + 7\text{Sa}(7k_x \frac{W}{2}) ], \text{ and} \end{aligned} \quad (\text{C.12})$$

$$H_W(f_x) = \mathcal{F}_{1D} \left\{ \frac{\text{Rect}\left(\frac{x}{W}\right)}{W} \right\} = \text{Sa}\left(k_x \frac{W}{2}\right) . \quad (\text{C.13})$$

A plot of the normalized two-dimensional spectrum, is shown in Figure C.2, where an angular width of the bars  $W=1$  mrad and a normalization factor of  $1/(28W^2)$  are used.

Figures C.3 and C.4 show the normalized spectrum expressed as a function of  $f'_x = f_x W$  (along the x-axis) and  $f'_y = f_y W$  (along the y-axis) respectively, for the same angular width and normalization factor as Figure C.2. This allows an estimation of the two-dimensional spectrum for different standard pattern sizes.

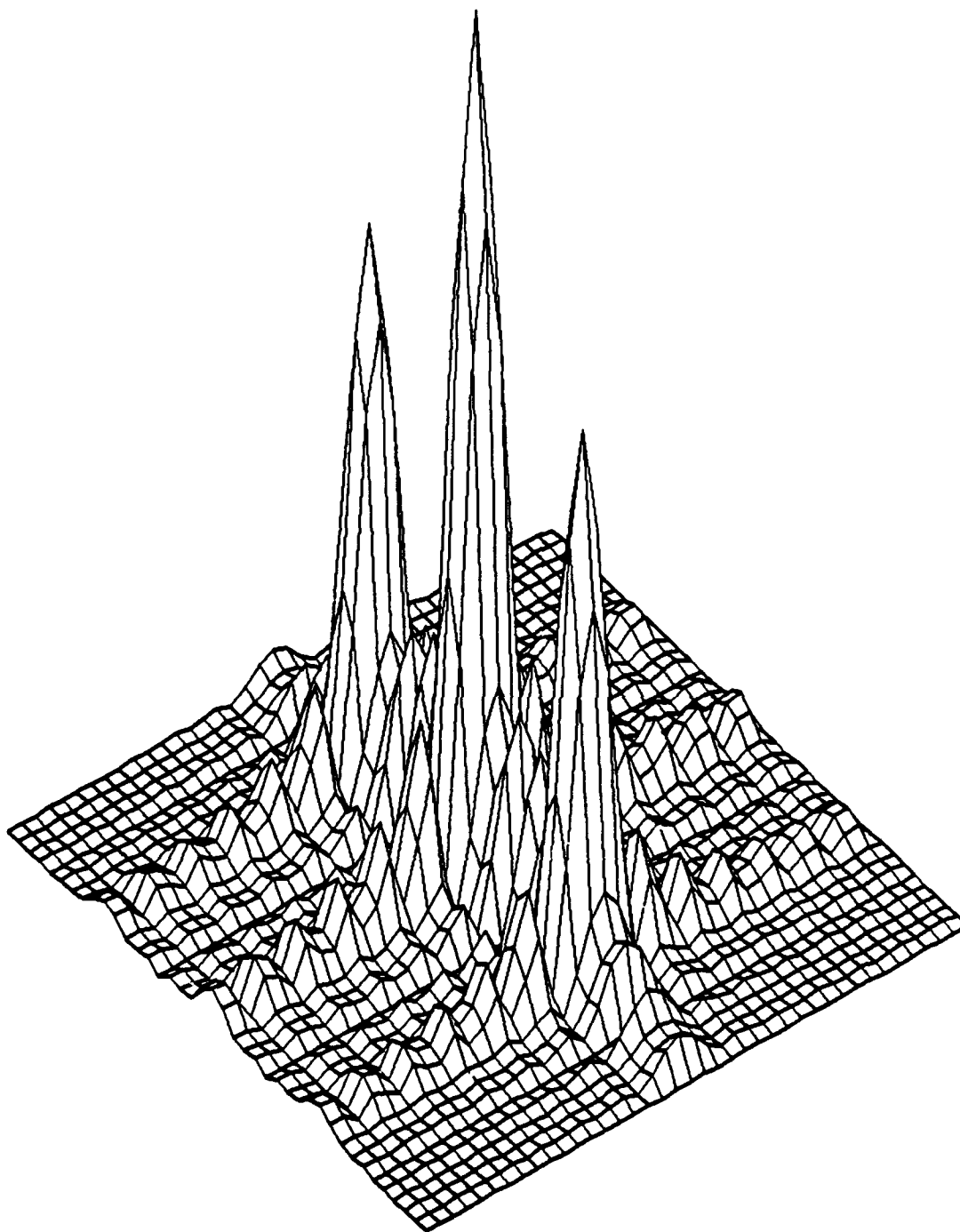


Figure C.2. Two-dimensional normalized target spectrum

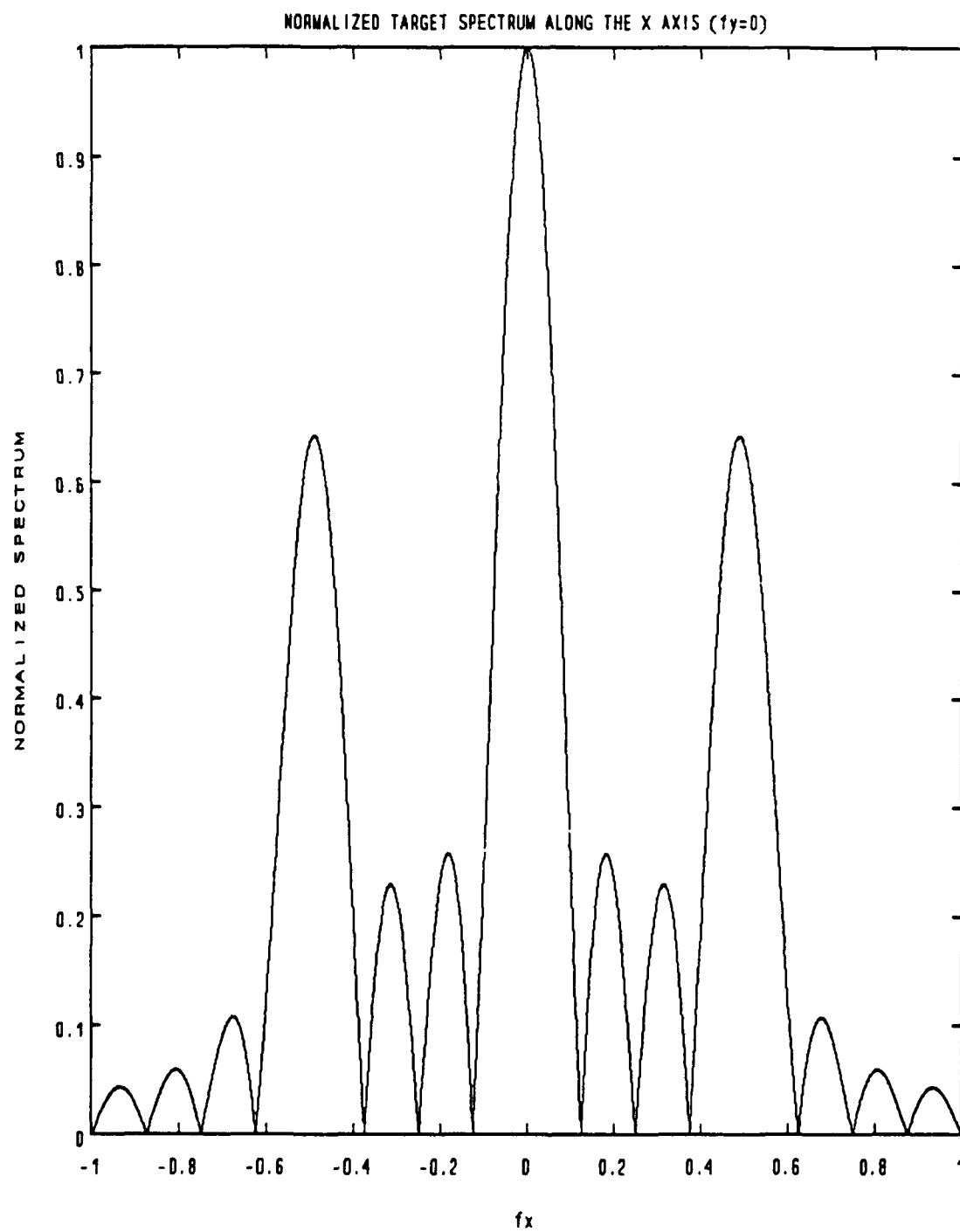


Figure C.3. Normalized target spectrum along the x-axis



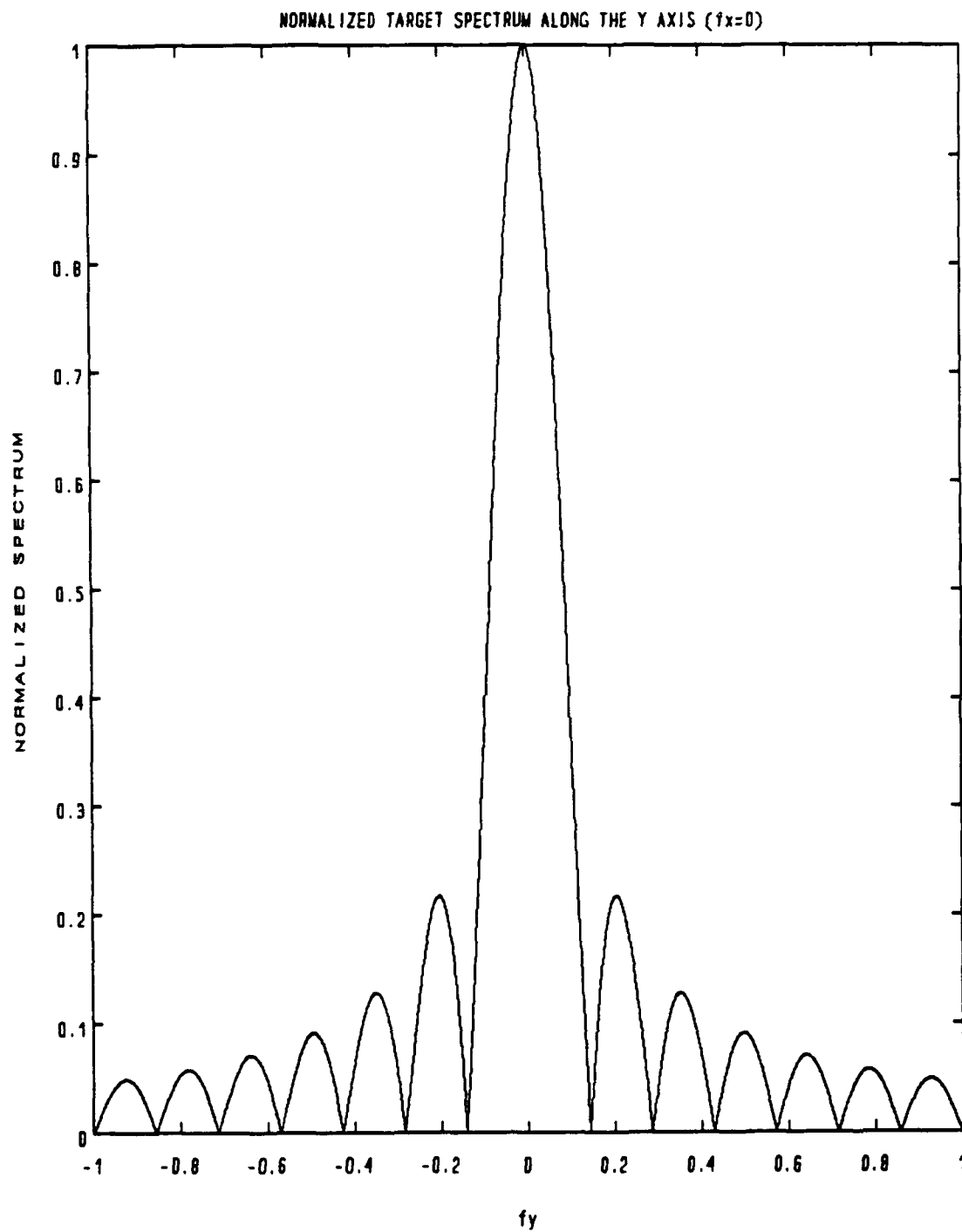


Figure C.4. Normalized target spectrum along the y-axis

#### APPENDIX D - SAMPLE SYSTEM

In order to simulate the different models of MRTD presented in this thesis, a sample system was selected in coincidence with the one employed by Lloyd [Ref. 10]. The parameters of that system are as follows:

Lens focal length ( $d$ )=.....50000  $\mu\text{m}$   
Diameter of lens ( $D$ )=.....20000  $\mu\text{m}$   
F/ number ( $F=d/D$ )=.....2.5  
Detector array individual element size (square)=.....0.005 cm  
Horizontal detector angular subtense ( $\Delta x$ )=.....1 mrad  
Vertical detector angular subtense ( $\Delta y$ )=.....1 mrad  
Detectors cold shielding scheme=.....not background limited  
Characteristic wavelength of the detectors ( $\lambda_p$ )=.....11.5  $\mu\text{m}$   
Spectral bandpass of detectors=.....8  $\mu\text{m}$  - 11.5  $\mu\text{m}$   
Specific detectivity at  $\lambda_p$  ( $D^*_{(\lambda_p)}$ )=..... $2 \cdot 10^{10}$  cm Hz<sup>1/2</sup>/watt  
Specific detectivity in the bandpass=..... $\lambda D^*_{(\lambda_p)} / \lambda_p$   
Frame rate ( $F_r$ )=.....30 Hz  
Scan rate format=.....60 fields/sec  
Number of detectors in parallel ( $n_p$ )=.....150  
Number of scan lines=.....300  
Interlace=.....2 to 1  
Horizontal scan efficiency ( $\eta_h$ )=.....0.8  
Vertical scan efficiency ( $\eta_v$ )=.....0.8  
Overall scan efficiency ( $\eta_{sc} = \eta_h * \eta_v$ )=.....0.64

Overscan ratio ( $\eta_{ovsc}$ ) = .....1  
 Distance between horizontal scan lines ( $\Delta y_i$ ) = .....1 mrad  
 Horizontal field of view (HFOV) = .....400 mrad  
 Vertical field of view (VFOV) = .....300 mrad  
 Detector dwell time ( $\tau_d = n * \eta_{sc} * X * Y / (HFOV * VFOV * Fr)$ ) = ..2.67\*10<sup>-5</sup> sec  
 Horizontal scanning velocity ( $v_x = X / \tau_d$ ) = .....37453.2 mrad/sec  
 3-dB frequency electronic roll-off ( $f_r$  in Hertz) = ...18716.6 Hz  
 3 dB frequency electronic roll-off ( $f_{rx}$  in cy/mrad) = 0.5 cy/mrad  
 CRT spot size parameter (a) = .....1.234  
 Noise equivalent reference bandwidth ( $\Delta f_n$ ) = .....29.4 Khz  
 S/N threshold for detection of one bar ( $\bar{\Psi}$ ) = .....4.5  
 Background temperature ( $T_g$ ) = .....300°K  
 Monochromatic wavelength of the target ( $\lambda$ ) = .....10  $\mu$ m  
 Optical efficiency of the viewer ( $\eta_{o(\lambda)}$ ) = .....0.8

## LIST OF REFERENCES

1. R. C. Braddick and J. H. Ludlow, "Assessing the performance of thermal imagers," Infrared Systems-Design and Testing, SPIE, Vol. 916, P.R. Hall and J. Seeley, eds., SPIE, Bellingham, Washington, pp. 84-91, 1988
2. G. W. Edwards, "Objective measurement of minimum resolvable temperature difference (MRTD) for thermal imagers," Image Assessment: Infrared and Visible, SPIE, Vol. 467, T. L. Williams, ed., SPIE, Bellingham, Washington, pp. 47-54, 1983
3. J. T. Wood, W. Bentz, T. Pohle, and K. Hepfer, "Specification of Thermal Imagers," Optical Engineering, Vol. 15, No. 6, pp. 531-536, 1976
4. J. G. Vortman and A. Bar-Lev, "Optimal electronics response for parallel thermal imaging systems," Optical Engineering, Vol. 23, No 4, pp.431-435, 1984
5. J. A. Ratches, W. R. Lawson, L. P. Obert, R. J. Bergemann, T. W. Cassidy, J. M. Swenson, "Night Vision Laboratory Static Performance Model For Thermal Viewing Systems," U.S.Army Electronics Command Report # 7043, Night Vision Laboratory, Fort Belvoir, Virginia, 1975
6. R. L. Sendall and F. A. Rosell, "Static Performance Model based on the Perfect Synchronous Integrator Model," in The Fundamentals of Thermal Imaging Systems, Naval Research Laboratory Report No. 8311 , F. Rosell and G. Harvey, eds., Naval Research Laboratory, Washington, D.C., pp. 181-203, 1979
7. W. McCracken and L. Wajsfelner, "MRTD as a figure of merit," Thermal Imaging, SPIE, Vol 636, I. R. Abel, ed., SPIE, Bellingham, Washington, pp. 31-35, 1986
8. J. G. Vortman and A. Bar-Lev, "Improved minimum resolvable temperature difference model for infrared imaging systems," Optical Engineering, Vol. 26, No. 6, pp. 492-498, 1987
9. M. L. Gao, M. A. Karim, S. H. Zheng, "Device nonspecific minimum resolvable temperature difference for infrared imaging systems characterization," Optical Engineering, Vol. 29, No. 8, pp. 905-910, 1990

10. J. M. Lloyd, Thermal Imaging Systems, Chapters 4, 5, and 10, Plenum Press, New York, 1975
11. F. A. Rosell and R. H. Willson, "Recent psychophysical experiments and the display signal-to-noise concept," in Perception of Displayed Information, L.M. Bieberman, ed., pp. 167-232, Plenum Press, New York, 1973
12. G. H. Kornfeld and W. R. Lawson, "Visual-Perception Models," J. Optical Soc. Am., Vol. 61, No. 6, pp. 811-820, 1971
13. A. D. Schnitzler, "Theory of spatial-frequency filtering by the human visual system. I. Performance limited by quantum noise," J. Optical Soc. Am., Vol. 66, No. 6, pp. 608-617, 1976
14. A. D. Schnitzler, "Theory of spatial-frequency filtering by the human visual system. II. Performance limited by video noise," J. Optical Soc. Am., Vol. 66, No. 6, pp. 617-625, 1976
15. F. W. Campbell, "The Human Eye as an Optical Filter," Proceedings of the IEEE, Vol. 56, No. 6, pp. 1009-1014, 1968
16. F. A. Rosell, "Video, Display, and Perceived-Image Signal-to-Noise Ratios," in The Fundamentals of Thermal Imaging Systems, Naval Research Laboratory Report No. 8311, F. Rosell and G. Harvey, eds., Naval Research Laboratory, Washington, D.C., pp. 49-83, 1979
17. S. Park and R. Schowengerdt, "Image sampling, reconstruction, and the effect of sample-scene phasing," Applied Optics, Vol. 21, No. 17, pp. 3142-3151, 1982
18. W. Wittenstein, J. C. Fontanella, A. R. Newbery, and J. Baars, "The definition of the OTF and the measurement of aliasing for sampled imaging systems," Optica Acta, Vol. 29, No. 1, pp. 41-50, 1982
19. W. D. Montgomery, "Sampling in imaging systems," J. Optical Soc. Am., Vol. 65, No. 6, pp. 700-706, 1975
20. W. Schneider and W. Fink, "Integral sampling in optics," Optica Acta, Vol. 23, No. 12, pp. 1011-1028, 1976
21. S. K. Park, R. Schowengerdt, and M. A. Kaczynski, "Modulation-transfer-function analysis for sampled image systems," Applied Optics, Vol. 23, No. 15, pp. 2572-2582, 1984

22. R. G. Driggers, G. D. Boreman, M. R. Wellfare, "Comparison of two frame noise calculations for infrared linescanners," Optical Engineering, Vol. 29, No. 7, pp. 781-785, 1990
23. T. L. Williams, N. T. Davidson, and S. Wocial, "Results of some Preliminary Work on Objective MRTD Measurement," Image Quality, An Overview, SPIE, Vol. 549, E. M. Granger and L. R. Baker, eds., SPIE, Bellingham, Washington, pp.44-49, 1985
24. G. Cuthberston, L. G. Shadrake, N. J. Short, "A technique for the objective measurement of MRTD," Infrared Technology and applications, SPIE, Vol. 590, L. R. Baker, A. Masson, eds., SPIE, Bellingham, Washington, pp.179-192, 1985
25. A. R. Newbery and R. McMahon, "Use of minimum resolvable temperature difference (MRTD) for the evaluation and specification of thermal imaging systems," Assessment of Imaging Systems: Visible and Infrared, SPIE, Vol. 274, T. L. Williams, ed., SPIE, Bellingham, Washington, pp. 268-272, 1981
26. T. L. Williams, "Assessing the performance of complete thermal imaging systems," Infrared Technology and Applications, SPIE, Vol. 590, L. R. Baker and A. Masson, eds., SPIE, Bellingham, Washington, 172-178, 1985
27. L. M. Biberman, Perception of Displayed Information, Plenum Press, New York, 1973.
28. J. A. Ratches, "Static Performance Model for Thermal Imaging Systems," Optical Engineering, Vol. 15, No. 6, pp.525-530, 1976
29. J. W. Goodman, Introduction to Fourier Optics, p. 127, McGraw-Hill, New York, 1968
30. W. R. Lawson and J. A. Ratches, "The Night Vision Laboratory Static Performance Model Based on the Matched Filter Concept, The Fundamentals of Thermal Imaging Systems, EOTPO Report No. 46, Appendix C, F. Rosell and G. Harvey, eds., pp.159-180, Electro-Optical Technology Program Office, Washington D.C., 1979
31. L. W. Couch II, Digital and Analog Communication Systems, p. 65, Macmillan Publishing Co., New York, 1990
32. F. G. Stremler, Introduction to Communication Systems, pp. 125-126, Addison-Wesley Co., Reading, MA, 1982

33. R. D. Hudson Jr., Infrared System Engineering, pp.305-310, John Wiley & sons, New York, 1969
34. W. Wolfe and G. Zissis, The Infrared Handbook, p. 15, Environmental Research Institute, Michigan, 1985
35. M. Spiegel, Schaum's Outline Series-Mathematical Handbook, McGraw-Hill, New York, 1968

# INITIAL DISTRIBUTION LIST

		No. of Copies
1.	Defense Technical Information Center Cameron Station Alexandria, Virginia 22304-6145	2
2.	Library, Code 52 Naval Postgraduate School Monterey, California 93943-5002	2
3.	Department Chairman, Code EC Department of Electrical and Computer Engineering Naval Postgraduate School Monterey, California 93943	1
4.	Chairman, Electronic Warfare Academic Group, Code EW Naval Postgraduate School Monterey, California 93943	1
5.	Professor Ron J. Pieper, Code EC/Pr Department of Electrical and Computer Engineering Naval Postgraduate School Monterey, California 93943	1
6.	Professor John P. Powers, Code EC/Po Department of Electrical and Computer Engineering Naval Postgraduate School Monterey, California 93943	1
7.	Comando de Operaciones Navales Edificio Libertad Comodoro Py 2055 Buenos Aires (1104) República Argentina	1
8.	Dirección General de Instrucción Naval Edificio Libertad Comodoro Py 2055 Buenos Aires (1104) República Argentina	1



- |     |   |   |
|-----|---|---|
| 9.  | Comando de la Flota de Mar<br>Edificio Libertad<br>Comodoro Py 2055<br>Buenos Aires (1104)<br>República Argentina           | 1 |
| 10. | Agregación Naval Argentina en los E.E.U.U.<br>Sr. Agregado Naval Argentino<br>630 Indiana Ave. NW,<br>Washington, DC, 20004 | 1 |
| 11. | Escuela de Oficiales de la Armada<br>Edificio Libertad<br>Comodoro Py 2055<br>Buenos Aires (1104)<br>República Argentina    | 1 |
| 12. | LT Alejandro R. Ugarte<br>Edificio Libertad<br>Comodoro Py 2055<br>Buenos Aires (1104)<br>República Argentina               | 2 |